Polygenic architecture of flowering time and its relationship with local environments in the grass *Brachypodium distachyon.*

Nikolaos Minadakis[1], Lars Kaderli[1], Robert Horvath[1], Yann Bourgeois[2], Wenbo Xu[1], Michael Thieme[1], Daniel P. Woods[3,4] and Anne C. Roulin[1*]

[1] Dept. of Plant and Microbial Biology, University of Zürich, Zollikerstr. 107, 8008 Zürich, Switzerland.
[2] DIADE, University of Montpellier, CIRAD, IRD, Montpellier, France.
[3] Department of Plant Sciences, University of California-Davis, 104 Robbins Hall Davis, CA 95616.
[4] Howard Hughes Medical Institute, Chevy Chase, Maryland, United States of America.

[*] **Corresponding author:** anne.roulin@botinst.uzh.ch

Abstract

Synchronizing the timing of reproduction with the environment is crucial in the wild. Among the multiple mechanisms annual plants evolved to sense their environment, the requirement of cold-mediated vernalization is a major process that prevents individuals from flowering during winter. In many annual plants including crops, both a long and short vernalization requirement can be observed within species, resulting in so-called early-(spring) and late (winter)-flowering genotypes. Here, using the grass model *Brachypodium distachyon*, we explored the link between flowering time-related trait (vernalization requirement and flowering time), environmental variation, and diversity at flowering-time genes by combining measurements under greenhouse and outdoor conditions. These experiments confirmed that *B. distachyon* natural accessions display large differences regarding vernalization requirements and

ultimately flowering time. We underline significant, albeit quantitative effects of current environmental conditions on flowering time-related traits. While disentangling the confounding effects of population structure on flowering time-related traits remains challenging, population genomics analyses indicate that well-characterized flowering-time genes may contribute significantly to flowering time variation and display signs of polygenic selection. Flowering-time genes, however, do not colocalize with GWAs peaks obtained with outdoor measurements, suggesting that additional genetic factors contribute to flowering time variation in the wild. Altogether, our study fosters our understanding of the polygenic architecture of flowering time in a natural grass system and opens new avenues of research to investigate the gene-by-environment interaction at play for this trait.

Key words: Flowering time, adaptation, vernalization, *B. distachyon*, grasses, polygenic selection.

Article Summary

Synchronizing the timing of reproduction with the environment is crucial in the wild. We used here the model *Brachypodium distachyon* to expand our knowledge on the adaptive potential and polygenic architecture of flowering time in wild grasses. While genetic factors play an important role in flowering time variation in our species, we showed that flowering time correlates with environmental variables and is therefore a locally adapted trait.

Introduction

The induction of reproduction is a critical fitness-related trait in the wild (Gaudinier and Blackman 2020), as a failure to produce offspring during the growing season may lead to the extinction of the individual's genotype. In many annual plant species adapted to temperate climates, plantlets establish themselves in the fall and overwinter before flowering and producing seeds in more favorable spring conditions (Chouard 1960; Blackman 2017). Vernalization, the prolonged exposure to cold necessary to render plants competent to flower (Chouard 1960), is hence a key component of plant reproduction as it prevents individuals from flowering prior to winter. The adaptive potential and the genetic architecture of flowering time has been studied in an unrivaled manner in *Arabidopsis thaliana* (for review Andrés and Coupland 2012; Blümel et al. 2015; Takou et al. 2019) due to the broad geographical distribution of the species and large genomic resources developed by the community (but see Hall et al. 2006; Monnahan and Kelly 2017; Yan et al. 2021 for works on other *Brassicaceae* and *Mimulus guttatus*). Vernalization is yet controlled by different genes in different plant groups and likely evolved independently multiple times during flowering plant diversification (Ream et al. 2012; Bouché et al., 2017; Raissig and Woods 2022). Moreover, specific crop flowering-time genes (e.g. *ID1* in maize) are for instance lacking homologs in *A. thaliana* (Blümel, Dally, and Jung 2015). As a wild monocot, the model for the temperate grasses *Brachypodium distachyon* constitute a prime system to study the evolution of flowering-time genes. In this context, we made use of the diversity panel developed for this species (Gordon et al. 2017; Gordon et al. 2020; Skalska et al. 2020;

68 Stritt et al. 2022, Minadakis et al. 2023) to expand our knowledge on the adaptive
69 potential and polygenic architecture of flowering time in grasses.

70 Initially established as a model for bioenergy crops (International Brachypodium
71 Initiative 2010), the grass species *B. distachyon* has more recently become a prime
72 model for developmental biology (Woods et al. 2017[a]; Woods et al. 2019; Nunes et al.
73 2020; Hasterok et al. 2022; Raissig and Woods 2022; Zhang et al. 2022; Slawinska et al.
74 2023), evolutionary genomics (Bourgeois et al. 2018; Gordon et al. 2020; Gordon,
75 Contreras-moreira, et al. 2017; Stritt et al. 2018; 2020; Eichten et al. 2016) and molecular
76 ecology (Del'Acqua et al. 2014; Wilson et al. 2019; Skalska et al. 2020; Stritt et al. 2022;
77 Minadakis et al. 2023). In addition to a chromosome-level genome assembly of 272
78 Mb (International Brachypodium Initiative 2010), a diversity panel composed of 332
79 accessions spanning from Spain to Iraq has been sequenced (Gordon et al. 2017;
80 Gordon et al. 2020; Skalska et al. 2020; Stritt et al. 2022, Minadakis et al. 2023), opening
81 new avenues of research in this system (Minadakis et al. 2023). We previously showed
82 that *B. distachyon* accessions cluster into three main genetic lineages (A, B and C),
83 which further divide into five main genetic clades: the ancestral C clade in Italy and
84 Balkans, the B_West clade in Spain and France, the B_East clade spanning from Turkey
85 to Caucasus and Iraq, the A_Italia clade in Italy as well as the A_East clade in Turkey
86 and Greece (Stritt et al. 2022, Minadakis et al. 2023). These natural accessions are found
87 in diverse habitats (Bourgeois et al. 2018; Minadakis et al. 2023) making *B. distachyon*
88 an ideal model to investigate how genetic and environmental factors interact to shape
89 traits.

90 *B. distachyon* accessions display large phenotypic variation with regard to flowering
91 time (e.g. Ream et al. 2014; Gordon et al. 2017; Woods et al., 2019; Sharma et al. 2017),
92 with some accessions requiring little to no vernalization to flower rapidly (early flow-
93 ering accessions) in certain photoperiods, while other accessions require a few weeks
94 to several months of vernalization in order to flower (late flowering accessions) (Ream
95 et al., 2014; Gordon et al., 2017; Woods et al., 2019). These flowering differences have
96 been described as potentially adaptive and responsible for population distribution ac-
97 cording to climate variation (Gordon et al. 2017; Woods et al. 2019; Skalska et al. 2020).
98 However, the extent to which variation in vernalization requirement and ultimately
99 flowering time correlates with local environmental conditions has yet to be formally
100 tested in this species. For instance, whether late-flowering genotypes, which require
101 long vernalization treatments, have been selected to complete their life cycle at a
102 slower rate to overcome harsher or longer winter, as observed in Swedish populations
103 of *A. thaliana* (Ågren et al. 2017), remains an open question.

104 In a Mediterranean species like *B. distachyon*, not all accessions might be exposed
105 to harsh winter and short cold periods might be sufficient to allow permissive flowering
106 in the wild. In this study, we hence decomposed flowering time into four flowering
107 time-related traits: the minimum threshold duration (MTD) of vernalization necessary
108 to be permissive for flowering, the number of day to flower when MTD is received, the
109 saturating threshold duration of vernalization above which no further reduction in
110 flowering time is gained and the fastest time for a given accession to flower from the
111 day plants after vernalization saturation. We combined measurements under

greenhouse and outdoor conditions and asked i) Do flowering time-related traits correlate with environmental variables and show signs of local adaptation? ii) What is the respective contribution of flowering time genes to flowering time-related trait variation? iii) Are known flowering-time genes contributing to flowering time variation in the wild?

Materials and Methods

Biological materials and genomic resources

The *Brachypodium distachyon* diversity panel is composed of 332 natural accessions for which whole-genome sequencing data are publicly available (Gordon et al. 2020; Gordon, Contreras-moreira, et al. 2017; Skalska et al. 2020; Stritt et al. 2022). For the flowering time experiment, we selected a subset of 61 accessions representing all five genetic clades as first described by Stritt et al. 2022 and occurring along latitudinal gradiants. Maps were drawn QGIS (version 3.16).

We also made use of the raw vcf produced by Minadakis et al. (2023) for the entire diversity panel. We used vcftools (Danecek et al. 2011) to apply the following filtering criteria: --max-alleles 2 --max-missing-count 200 --minQ 20. We further filtered heterozygous SNPs as those have been shown to result from duplicated sequenced and be mostly artifactual in selfing species (Stritt et al. 2022). All the analyses were performed on version3 of the *B. distachyon* genome (https://phytozome-next.jgi.doe.gov).

134 **Flowering time-related trait measurements**

135 We performed an experiment in controled conditions from October 2021 until May
136 2022 in order to test the flowering phenology of the five genetic clades of
137 *Brachypodium distachyon.* Twelve accessions per genetic clade were selected, in addi-
138 tion to the reference accession Bd21. All accessions were treated with five vernalization
139 periods spanning from 2 to 10 weeks, with three replicates per treatment and per
140 accession. Seeds were stratified for at least two weeks before the experiment, and then
141 sowed in pots that were placed in greenhouse conditions (16 h day at 20°C and 8 h
142 dark at 18°C with a light intensity of 200 µMol/m2/s). We distributed the replicates
143 randomly across trays to minimize bias due to position effects. Three weeks after
144 germination the plants were transfered to a cooling chamber (constant temperature
145 at 4°C, 8h light 80 µMol/m2/s, and 16 h dark) for 2, 4, 6, 8, and 10 weeks. At the end
146 of the vernalization treatment, plants were moved back to the greenhouse.

147 Flowering time was measured as the number of days after return to greenhouse to
148 the first day of spike emergence which is consistent with stage 50 of the Zadoks scale
149 that was used in (Ream et al. 2014). Measurements were taken every two days until the
150 end of the experiment in May. During the experiments, trays were permuted on the
151 table to further limit position effects.

152 We then extracted from this experiment four flowering time-related traits: i) the
153 minimum threshold duration of vernalization necessary to be permissive for flowering,
154 ii) the number of day to flower when the minimum threshold is received, iii) the satu-
155 rating threshold duration of vernalization above which no further reduction in

flowering time is gained and, iv) the fastest time for a given accession to flower from the day plants were moved to the vernalization chamber, i.e. the number of day to flower when vernalization saturation is received. This latter trait is classically used as a measure of flowering time in *B. distachyon* studies. Results were plotted in R version 4.0.2 (R Core Team, 2018) with the package ggplot2 (Wickham 2016).

Extraction of current and past bioclimatic variables

Raster maps for current monthly solar radiation and altitude were retrieved from worldclim (https://www.worldclim.org). In addition, raster maps for monthly Global Aridity Index (GAI) were obtained from https://cgiarcsi.community/data/global-aridity-and-pet-database/. Bioclimatic variables were then extracted using the R packages raster (v.3.5-2, Hijmans & van Etten, 2012) and rgdal (v.1.5-27, Keitt et al., 2010) for each of the 332 accessions. For solar radiation and GAI, data were also average over spring months (April to June).

For paleo-bioclimatic variables, we used the niche suitability projections for the last glacial maximum (LGM) computed by Minadakis et al (2022). For each genetic clade, we extracted the coordinates of a set of 200 random points per clade in highly suitable habitats (>0.85) with the raster package function rasterToPoints. We retrieved raster maps for LGM from https://www.worldclim.org/data/v1.4/paleo1.4.html and extracted the 19 paleo-bioclimatic variables for the corresponding sites as described above.

178 **Redundancy analysis (RDA)**

179 We extracted the 19 classical bioclimatic variables as well as elevation, aridity and solar
180 radiation in spring for the 56 accessions for which flowering time-related trait were
181 measured. We performed a principal component analysis (PCA) with the R base func-
182 tion prcomp using the resulting 22 variables.

183 Association between flowering time-related traits, bioclimatic variables and genetic
184 cluster of origin were tested with redundancy analysis (RDA) using the R package Ve-
185 gan 2.6-4 (O'Hara et al. 2022) following (Capblancq and Forester 2023). RDA computes
186 axes that are linear combinations of the explanatory variables. In other words, this
187 method seeks, in successive order, a series of linear combinations of the explanatory
188 variables that best explain the variation of the response matrix (Borcard, Gillet and
189 Legendre 2018). It is therefore especially suited when explanatory variables are corre-
190 lated.

191 To identify which variable influence flowering time-related traits, we opted for a
192 forward selection approach (Capblancq and Forester 2023) and first ran empty models
193 where the respective flowering time-related trait were treated independently as a re-
194 sponse variable and explained by a fixed intercept alone. We then ran additional mod-
195 els where each flowering time-related traits were treated independently as a response
196 variable while the cluster of origin, the 22 environmental variables mentioned above
197 or both the cluster of origin and the 22 environmental variables were successively en-
198 tered as explanatory variables. These full models were compared to their respective

199 empty models with the Vegan ordiR2step function (Capblancq and Forester 2023) and
200 the following parameters: permutations = 1000, R2scope = T, Pin = 0.01.

201 We also tested for associations between flowering time and SNPs in known flower-
202 ing-time genes using RDA. To do so, we first extracted and converted the SNPs located
203 in flowering-time genes as a dataframe with vcftools -- bed --extract-FORMAT-info
204 GT, where the bed file contained the position of flowering-time genes. We first fitted
205 simple models where each flowering time-related traits were treated independently as
206 a response variable and all SNPs individually as explanatory variables. here again, we
207 compared those models with their respective empty models with the Vegan
208 ordiR2step function. For data visualization, the SNPs were pruned to remove SNPs in
209 perfect linkage disequilibrium within each gene with plink (Purcell et al. 2007) with the
210 following paramters --indep-pairwise 50 5 1. We kept one focal SNP per gene display-
211 ing the strongest association with one of the flowering time-related traits for further
212 analysis. In a second step, we fitted models where all focal SNPs were treated as ex-
213 planatory variables together. We eventually fitted full model where the cluster of origin
214 together with all focal SNPs and bioclimatic variable associated with the given flower-
215 ing time-related trait were treated as explanatory variables. All the plots were pro-
216 duced with the R package ggplot2.

217

218 **F_{ST} calculation**

219 Single SNP F_{ST} between accessions of the A and B lineages were calculated with
220 vcftools (Danecek et al. 2011). To account for shifts in the observed F_{ST} values caused

221 by the population structure of *B. distachyon*, the expected F_{ST} distribution under neu-
222 tral evolution was also estimated using forward simulations run in SLiM version 3.4
223 (Haller and Messer 2019). The population structure, effective population sizes and time
224 of divergences between lineages of *B. distachyon* during its evolution were modeled
225 in SLiM based on the results of Minadakis et al. (2023). No migration between the
226 different populations in the simulations was allowed, as a lack of interbreeding be-
227 tween the distinct *B. distachyon* clades was reported (Stritt et al. 2022). The simulation,
228 was run 100 times and single SNP F_{ST} were calculated for each simulation to generate
229 the expected F_{ST} distribution under neutrality.
230

231 **Linkage disequilibrium analyses**

232 To plot linkage disequilibrium (LD) decay, we first thinned the vcf with vcftools --thin
233 20000 to keep one SNP every 20 kilobases (kb). Intrachromosomal LD (r^2) was calcu-
234 lated with vcftools --geno-r2. We repeated this step by further filtering the vcf for a
235 minimum allele frequency of 0.05 with vcftools -- maf 0.05. For both outputs, we vis-
236 ualized LD decay by plotting r^2 and its 95 CI as a function of the physical distance
237 between SNPs with the R package ggplot2. LD between focal SNPs in flowering-time
238 genes was calculated separately with vcftools –geno-r2 and added to the LD decay
239 plot for comparison. LD plots for focal SNPs were produced with the R package gaston
240 (Pedry and Dandine-Roulland 2020).

241 Inter-chromosomal LD (r^2) was calculated with vcftools --interchrom-geno-r2 for a
242 subset of 100,000 loci selected randomly in the genome. We then re-sampled 50,000

243 times different combination of loci and calculated the mean LD each time. This allowed
244 us to further calculate the CI around the mean and compare our real data to this dis-
245 tribution.
246
247 **Scans of selection**
248 The X^TX analysis was performed with BayPass v2.3 using the five genetic clades or three
249 genetic lineages as populations (Gautier 2015). We generated the input file by using
250 vcftools --count to calculate the allele frequency of each SNP present in our vcf (no
251 filtering on minor minimum allele frequency). We then ran Baypass on our actual da-
252 taset with the following parameters: -pilotlength 500 -npilot 15 -burnin 2500 -nthreads
253 6. To calibrate the X^TX and define a threshold of significance for differentiated SNPs,
254 we then used the simulate.baypass function from baypass_utils (Gautier et al. 2015) to
255 generate a pseudo-observed dataset (POD) of 100,000 loci based on the co-variance
256 matrix computed with our real dataset. We then ran Baypass on the POD with the
257 parameters described above. We used the 0.99 quantile of the X^TX calculated for the
258 POD as a threshold of significance for the real dataset. Integrated Haplotype Scores
259 (IHS) were also computed for accessions of the A and B lineages separately with the R
260 package Rehh 3.1 (Gautier et al. 2017)
261
262
263

264 **Functional effect and age estimates of variants**

265 The functional effect of variants was annotated using SnpEff version 5.0e (Cingolani et
266 al. 2012) using default parameters and the provided database for *Brachypodium*
267 *distachyon*.

268 The age of each single SNP was computed with GEVA (Albers and McVean 2020) to
269 estimate the average SNP age for each annotated gene (https://phytozome-
270 next.jgi.doe.gov) in the derived A and B genetic lineages as well as in the five genetic
271 clades. All private SNPs to the combined A and B lineages were polarized using the
272 ancestral C lineage using custom R scripts. GEVA was run on the five main scaffolds
273 (corresponding to the five chromosomes) using the genetic map produced by (Huo et
274 al. 2011) and the polarized SNP dataset.

275

276 **Genome-wide association analysis**

277 We further used the flowering time measurements performed outdoor in Zurich in
278 2017 (Stritt et al. 2022). We extracted the 19 classical bioclimatic variables as well as
279 altitude, aridity and solar radiation for the 332 accessions as well as a site in Zurich (lat
280 = 43.73693085, lon = 3.69295907) and performed a principal component analysis
281 (PCA) as described above. Linear-mixed model analyses were performed as described
282 above for the greenhouse experiment.

283 To identify loci associated with flowering time variation, we performed a genome-
284 wide association analysis with GEMMA (Zhou and Stephens 2012). Due to population
285 structure, we corrected the analysis by a centered relatedness matrix, first produced

286 with the option -gk 1. Association tests were performed using the option -maf 0.05 to
287 exclude SNPs with minor allele frequency with values less than 0.05. Regions were con-
288 sidered significantly associated if displaying at least four markers above FDR threshold
289 in 8Kb windows (overlap of 4Kb). Upset plots were drawn with the R package UpSetR
290 (Gehlenborg 2019).
291

292 **Overlaps with Environmental association analyses**

293 We made use of the environmental association analyses performed by Minadakis et al.
294 (2023) to assess whether flowering-time genes and the candidate gene identified by
295 the GWAs were associated with current environmental variables. Upset plots were
296 drawn in R with the R package UpSetR (Gehlenborg 2019).
297

298 **Gene duplication**

299 We checked for potential gene duplication with detettore
300 (https://github.com/cstritt/detettore), a program developed to study structural varia-
301 tion based on short-read sequences (Stritt 2021). We also calculated the proportion of
302 heterozygous sites over the 22 flowering-time genes and 332 accessions, using the
303 raw vcf produced by Minadakis et al. (2023) not filtered for heterozygous SNPs but
304 with the following criteria: --max-alleles 2 --max-missing-count 200 --minQ
305
306
307

308 # Results

309 ## Flowering time measurements under greenhouse conditions

310 We selected 61 accessions (Figure 1A) from the *B. distachyon* diversity panel (Minada-
311 kis et al. 2023) for our flowering time experiment. Those accessions were chosen to
312 represent all five genetic clades and occur, when possible, along latitudinal gradients.
313 Briefly, we submitted plants to five vernalization treatments (2, 4, 6, 8 or 10 weeks at
314 4°C) with three replicates each and measured how long plants took to flower after the
315 return to warm conditions (Figure S1, Table S1 for the raw data). For five out of the 61
316 accessions (Veg12 from A_East; Ren4, Lb1, Lb23 and Cm7 from A_Italia), none of the
317 replicates flowered by the end of the experiment (Figure 1a, Figure S1) despite normal
318 growth. All subsequent analyses were hence performed on the 56 accessions for which
319 flowering time data were collected.

320 However, *B. distachyon* accessions span a large range of habitats (Minadakis et al.
321 2023). While some accessions of the diversity panel can experience up to -11 °C as a
322 minimum temperature during the coldest months (Bio6), the mean temperature during
323 the coldest quarters (Bio11) is above 4 °C for a large number of accessions (Table S2,
324 Figure S2). As such, not all accessions may experience long vernalization at 4 °C in the
325 wild. We thus extracted four traits link to vernalization requirements and *in fine* flow-
326 ering time (Table S3) for further analyses: i) the minimum threshold duration of ver-
327 nalization necessary to be permissive for flowering (hereafter MTD), ii) the number of
328 day to flower when MTD is received (hereafter day to flower after MTD), iii) the satu-
329 rating threshold duration of vernalization above which no further reduction in

330 flowering time is gained (hereafter vernalization saturation) and, iv) the fastest time for
331 a given accession to flower from the day plants were moved to the vernalization cham-
332 ber, i.e. the number of day to flower when vernalization saturation is received (hereaf-
333 ter day to flower after vernalization saturation). Note that all plants germinated within
334 5 days and germination time was therefore not included for further analyses.

335 Flowering-related traits show significant albeit moderate correlation among each
336 other (Figure 1b) and, with the exception of day to flower after MTD, a partitioning of
337 the phenotypes per genetic clades (Figure 1c and Table S4 for P-values). Accessions
338 from the C, B_East and B_West clades show a significantly reduced MTD compared to
339 accessions from the A_East and A_Italia clades. Accessions from the B_East and B_West

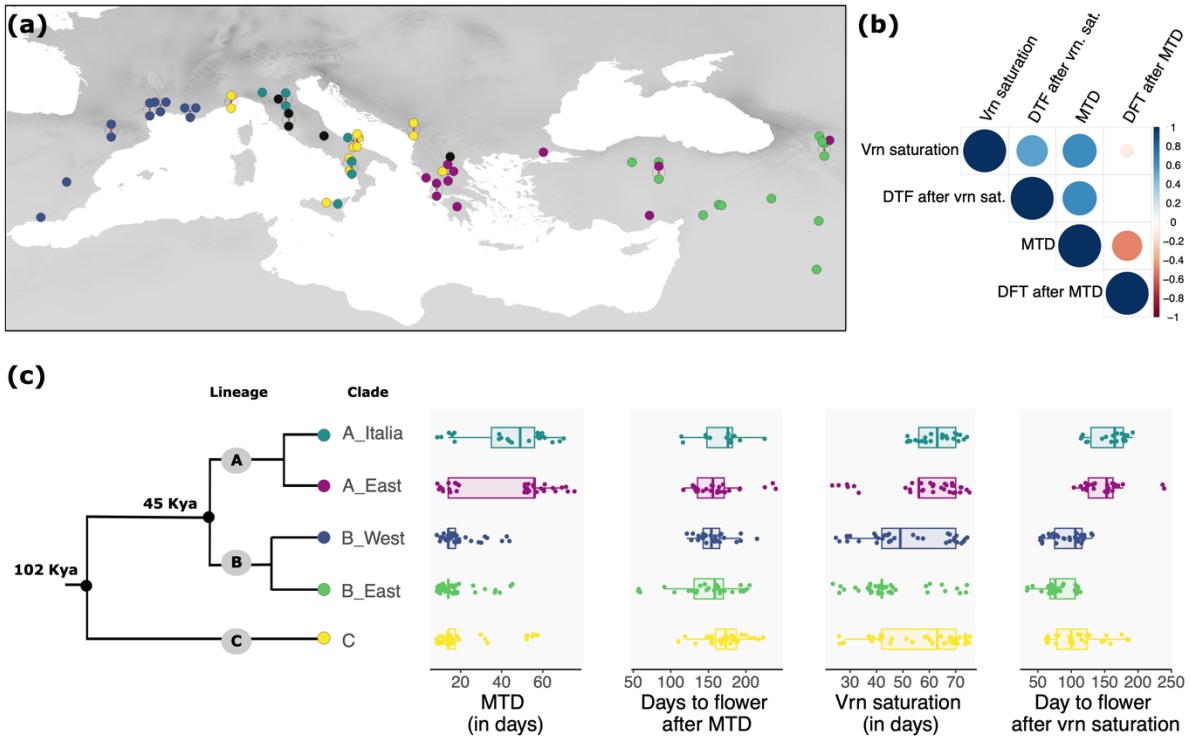

Fig. 1: Geographical origins of the samples used for greenhouse experiment and flowering time-related trait variation. (a) Map displaying the location of a given accession as well as their genetic clade of origin (C in yellow, A_East in magenta; A_Italy in turquoise; B_East in green and B_West in dark blue). Accessions that did not flower by the end of the experiment are depicted in black. (b) Correlogram of the four flowering time-related traits among accessions (Pearson correlation assuming linear relashionship). DFT: day to flower; MTD: minimum threshold duration of vernalization (c) Schematic phylogeny and distribution of the four flowering time-related traits.

340 also tend to show a shorter saturating threshold duration of vernalization compared
341 to accessions from the three other clades (Figure 1c and Table S4). Eventually, acces-
342 sions from the C, B_East and B_West clades flower significantly faster when vernaliza-
343 tion is saturated (Figure 1b and Table S4). Altogether, these results reflect that acces-
344 sions from the A lineage display overall a longer life cycle (late-flowering genotypes)
345 than the ones from the B and C lineages (early-flowering genotypes) due to longer
346 vernalization time requirements but longer time to flower after the return to warm
347 conditions (Figure S1).

348

349 **Association between flowering time-related traits and bioclimatic variables.**

350 To test whether flowering time-related traits correlate with environmental variation,
351 we extracted the 19 classical worldclim bioclimatic variables (Bio1 to Bio19) as well as
352 solar radiation in spring, global aridity index in spring and altitude for each locality and
353 performed a PCA with the resulting 22 variables (Table S3). The first two axes of the
354 PCA explained together about 58% of the variation among our samples, indicating that
355 our set of selected accessions occur in different environmental conditions.

356 We have previously shown that the five *B. distachyon* occur in different ecological
357 niches (Minadakis et al. 2023) leading to a confounding effect of population structure
358 and environmental variation. As mentioned above, we also observed in the current
359 study some partitioning of the phenotypes per genetic clades for the flowering time-
360 related traits we investigated. Eventually, most bioclimatic variables display correlation

among each other in our system (Minadakis et al. 2023, Figure S3). We therefore used a redundancy analysis (RDA) to test for associations between flowering time-related traits and bioclimatics variables, as this approach typically accounts for confounding factors by maximizing the genetic variance explained by a set of environmental predictors.

Specifically, to model the relationships among flowering time traits, bioclimatic variable and population structure, we fitted models where flowering time-related traits were independently entered as response variable while the cluster of origin (model = cluster alone), the 22 environmental variables (model = all bioclimatic variables) or both the cluster of origin and the 22 bioclimatic variables (model = cluster + all bioclimatic variables) were successively entered as explanatory variables. We compared those full-models to empty models where the respective flowering time-related trait was explained by a fixed intercept alone (Capblancq and Forester 2023).

Consistent with the phenotype distributions (Figure 1b), the genetic cluster of origin alone contribute to MTD (R^2 = 0.25), day to flower after vernalization saturation (R^2 = 0.44) and vernalization saturation (R^2 = 0.1) but not to day to flower after MTD (Table1). We found that a large part of the variance in flowering time-related traits is explained by bioclimatic variables (precipitation levels and temperature) linked to warm months but only marginally by elevation or variables linked to cold month (e.g. bio19; Table 1) when the models did not include the cluster of origin. Eventually, environmental (bioclimatic variables) still explained a significant part of the variance in flowering time-

Table1: RDA output for each flowering time-related trait and outdoor experiment

Trait	Model	Variable	Cumulative R2adj	AIC	F	P-value
MTD	cluster alone	cluster	0.25	248.18	11.35	0.002
	All bioclim variables	bio18	0.18	256.40	28.29	0.002
		bio16	0.22	250.64	7.81	0.006
		bio13	0.28	243.22	9.47	0.004
		all variables	0.45			
	Cluster + all bioclim variables	cluster	0.25	248.18	11.35	0.002
		bio18	0.42	218.35	34.53	0.002
		elevation	0.46	210.31	9.88	0.002
		all variables	0.58			
Day to flower after MTD	cluster alone	cluster	-	-	-	NS
	All bioclim variables	aridity_spring	0.26	15.07	45.31	0.002
		bio9	0.30	10.32	6.77	0.006
		bio5	0.33	5.08	7.21	0.01
		bio18	0.37	-0.46	7.46	0.006
		all variables	0.52			
Vernalization saturation	cluster alone	cluster	0.10	126.14	4.31	0.004
	All bioclim variables	aridity_spring	0.22	105.17	35.61	0.002
		elevation	0.27	98.59	8.66	0.004
		all variables	0.42			
	Cluster + all bioclim variables	aridity_spring	0.22	105.17	35.61	0.002
		elevation	0.27	98.59	8.66	0.006
		all variables	0.44			
Day to flower after veranlization saturation	cluster alone	cluster	0.44	108.19	25.53	0.002
	All bioclim variables	aridity_spring	0.31	132.17	56.02	0.002
		bio16	0.39	116.82	18.17	0.002
		all variables	0.54			
	Cluster + all bioclim variables	cluster	0.44	108.19	25.53	0.002
		aridity_spring	0.60	68.74	46.84	0.002
		bio13	0.65	51.19	19.98	0.002
		bio16	0.68	42.35	10.60	0.002
		srad_spring	0.69	37.56	6.47	0.004
		all variables	0.78			
Day to flower (outdoor experiment)	cluster alone	cluster	0.38	2347.00	93.32	0.002
	All bioclim variables	bio18	0.42	2309.20	428.44	0.002
		bio12	0.45	2276.00	36.18	0.002
		bio19	0.51	2214.60	66.43	0.002
		all variables	0.60			
	Cluster + all bioclim variables	bio18	0.42	2309.20	428.44	0.002
		cluster	0.48	2243.40	19.46	0.002
		bio12	0.53	2188.60	58.93	0.002
		bio19	0.56	2146.50	45.21	0.002
		all variables	0.66			

bio18 : Precipitation of Warmest Quarter ; bio9: Mean Temperature of Driest Quarter; bio5: Max Temperature of Warmest Month; bio13: Precipitation of Wettest Month; bio16: Precipitation of Wettest quarter; bio12 : Annual Precipitation; bio19 : Precipitation of Coldest Quarter. We only display predictors that increase the cumulative R^2 by more than 0.03 while "all variable" display the cumulative R^2 explained by all significant predictors together.

382 related traits (Table 1) even in the full model including also the genetic clade of origin

383 (model clutser + all bioclimatic variables). This indicates that flowering time-related

384 traits, when measured under greenhouse conditions, are significantly shaped by the
385 current environmental conditions we tested in *B. distachyon* and are locally adapted
386 trait.

387 Note that variable selection optimizes the variance explained by explanatory varia-
388 bles but does not necessarily identify the ecological drivers of phenotypic variation. In
389 our system, where bioclimatic variables are highly correlated with each other and
390 sometimes with the genetic clade of origin (Figure S2), while one variable may maxim-
391 ize the variance, another one maybe the mechanistic driver of variation (Capblancq
392 and Forester 2023). As such, it remains difficult to disentangle the effect of the cluster
393 of origin from the effect of the environment for MTD and day to flower after vernali-
394 zation saturation (Table 1) and to estimate the actual part of the variance explained by
395 the environment for those two traits.

396 It is yet clear that accessions from more arid environments tend to flower faster
397 once vernalization saturation has been reached. Indeed, kendall rank correlations be-
398 tween flowering time and aridity in spring or annual precipitation levels (bio12) for
399 instance show a significant (P-value = 7.143e-06 and 4.982e-11 respectively) but only
400 partial correlations (Tau = -0.25 and 0.36 respectively), implying that while local envi-
401 ronment are driving flowering time variation and flowering time-related trait at large
402 (Table 1), it only partly explains the early/late-flowering partitioning of the phenotypes
403 we observe among genetic lineages (Figure 1c).

404

405 **Contribution of flowering time genes to flowering time-related trait variation**

406 The genetic basis of flowering time has been extensively characterized at the molecular
407 level in *B. distachyon* (e.g. Raissig and Woods, 2022; Woods et al., 2023). In a second
408 step, we also aimed to assess the contribution of genetic factors to flowering time-
409 related traits. Due to our relatively small sample size (56 accessions with phenotypes),
410 we opted for a targeted approach rather than a classical GWAs and selected 22 flow-
411 ering-time genes (Table S5) molecularly characterized and described as impacting
412 flowering time in our study system (Higgins et al. 2010; Wu et al. 2013; Woods et al.
413 2014; Sharma et al. 2017; Woods et al. 2017[a,b]; Lomax et al. 2018; Qin et al. 2019; Woods
414 et al. 2019; Cao et al. 2020; Kennedy and Geuten 2020; Woods et al. 2020).

415 Using the SNP calling performed by Minadakis et al. (2023), we extracted 502 SNPs
416 across these 22 flowering-time genes and 56 accessions and performed stepwise RDA.
417 We first fitted models where flowering time-related traits were independently entered
418 as response variable and each of the 502 SNPs were entered independently as explan-
419 atory variables. Here again, those models were compared to empty models where the
420 respective flowering time-related trait was explained by a fixed intercept alone. 302
421 SNPs across 20 flowering-time genes were significantly associated with at least one of
422 the four flowering time-related traits (Table S6). Due to linkage disequilibrium over
423 short distances (Figure S4a), many SNPs gave precisely the same signal of association
424 within a given gene (Table S6). We thus pruned our dataset. Overall, the resulting 143
425 SNPs show a strong association with day to flower after vernalization saturation and
426 MTD but very mild association with the two other traits (Figure 2a). Individual SNP

explained as much as 42% of the variance in day to flower after vernalization saturation (Table S6 and Figure 2b). SNPs in *VERNALIZATION1* (*VRN1*), *FLOWERING LOCUS T-LIKE 1* and *10* (*FTL1* and *FTL10*) and *POLD3* show the strongest association with day to flower after vernalization saturation and MTD (Figure 2a and b). Interestingly, *VRN1* and *VERNALIZATION2* (*VRN2*), two genes known to play a role in vernalization requirement, show a stronger association with MTD than with vernalization saturation (Figure 2a).

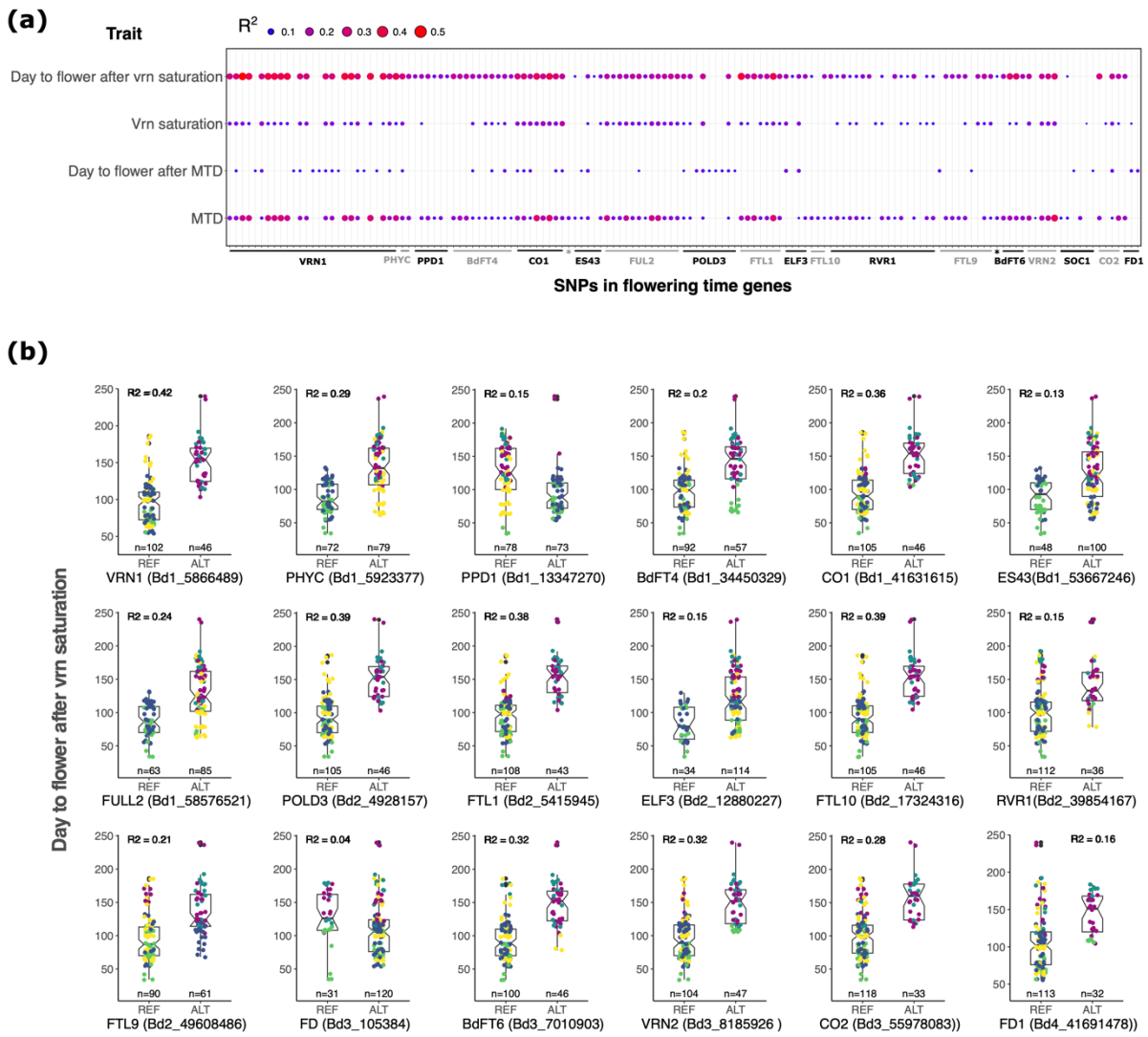

Fig. 2: Association between SNPs in flowering-time genes and flowering time-related traits. (a) RDA output for the 143 pruned SNPs. (b). For each gene, the boxplots contrast the effect of the reference (Bd21) and alternative alleles on day to flower after vernalization saturation for the SNP showing the strongest association with the trait. The color code is the same as in Figures 1.

434 Because SNPs in flowering-time genes show a marginal association with vernaliza-
435 tion saturation and day to flower after MTD, we focused on day to flower after vernal-
436 ization saturation and MTD for the rest of the analysis. To further disentangle the os-
437 tensible confounding effect of population structure (Figure 2b), SNPs in flowering-time
438 genes and environmental variables on day to flower after vernalization saturation and
439 MTD, we fitted additional models that included the phenotype as a response variable
440 and i) the cluster of origin alone (model = cluster alone), ii) all the 20 SNPs (1 SNP per
441 gene, figure S4b) showing the strongest association with either day to flower after
442 vernalization saturation or MTD (model = All SNPs) and, iii) the cluster of origin, all the
443 20 SNPs and the environmental variables associated with each respective trait (as
444 shown in Table1) as explanatory variables (model = cluster + all SNPs + envt.). We
445 compared these models successively with the empty model as previously described.
446 For both traits, single SNPs (e.g. Bd1_5866489 in *VRN1* for day to flower after ver-
447 nalization saturation and Bd2_5415945 in FTL1 for MTD) gave separately identical or
448 similar association as the cluster of origin alone (Table 2). This results in a reduced or
449 null cluster effect in the full model compared the one of single SNPs (Table 2). Note
450 that the variance explained by a given SNP (e.g. Bd1_5866489 in *VRN1*) differ from the
451 one obtained above (Figure 2b). RDA do not allow missing value and the models with
452 20 SNPs (Table2) are therefore based on a slightly different sample size than the model
453 performed with single SNP (Figure 2b) which results in different R^2 estimates.

Table 2: Output of the RDA between flowering time-related trait, SNPs in flowering time genes and bioclimatic variables

Trait	Model	Variable	Cumulative R2adj	AIC	F	P-value
Flowering time after vernalization saturation	cluster alone	cluster	0.56	10.72	26.44	0.002
	All SNPs	Bd1_5866489	0.56	7.58	103.39	0.002
		Bd3_8185926	0.58	4.51	5.04	0.01
		all variables	0.68			
	Cluster + SNPs + aridity_spring + bio13	Bd1_5866489	0.56	7.58	103.39	0.002
		aridity_spring	0.65	-10.08	21.41	0.002
		bio13	0.69	-18.38	10.44	0.002
		Bd2_5415945	0.72	-25.66	9.22	0.002
		Bd4_41691478	0.75	-35.32	11.62	0.004
			0.87			
MTD	cluster alone	cluster	0.32	132.53	10.57	0.002
	All SNPs	Bd2_5415945	0.37	123.86	48.04	0.002
		all variables	0.57			
	Cluster + SNPs + elevation + bio18	Bd2_5415945	0.37	123.86	48.04	0.002
		bio18	0.46	112.20	14.32	0.002
		cluster	0.52	105.56	3.66	0.008
		Bd3_8185926	0.57	98.44	8.71	0.006
		all variables	0.61			

As mentioned above, RDA optimize the variance explained but do not allow to identify the mechanistic driver of variation. Considering the allele distribution of SNPs in flowering time-genes across genetic cluster (Figure 2a), disentangling and quantifying the effect of population structure from the one of genetic factors or single gene remains therefore challenging for most SNPs in flowering time-genes.

Differentiation of flowering time genes

Most SNPs in flowering-time genes nonetheless appear to be highly differentiated among genetic clades. This could result from two processes. On the one hand, *B. distachyon* populations underwent bottlenecks during the last glaciation (Minadakis et al. 2023), which may have led to reduced genetic diversity and highly differentiated alleles among genetic lineages/clades genome-wide (neutral scenario). On the other hand,

466 flowering-time genes might be under positive selection and therefore highly differen-
467 tiated among genetic clades (selection scenario).

468 To first assess the extent to which our SNPs of interest are more differentiated com-
469 pared to genome-wide levels, we computed single SNP F_{ST}. To limit the number of
470 comparison and considering the partitioning of the reference and alternative alleles
471 among accessions in the flowering-time genes (Figure 2b), we only computed F_{ST} be-
472 tween accessions of the A and B lineages. We found that the large majority of SNPs
473 significantly associated with flowering time are above the 3rd quartile of the genome-
474 wide distribution or even belong to the top 5% outliers (Figure 3a). Hence, with the
475 exception of SNPs in *EARLY FLOWERING 3* (*ELF3*), *FD*, and *FD1*, all flowering-time
476 genes harbor SNPs that tend to be more differentiated than the rest of the genome.

477 To gain power for our analyses, we further made use of the *B. distachyon* diversity
478 panel composed of 332 natural accessions (Minadakis et al. 2023, Figure 4a) and found
479 very similar levels of allele differentiation at flowering-time genes (Figure S4c). These
480 results are in line with a forward simulation we performed under a neutral scenario
481 using the demographic estimates computed by Minadakis et al. (2023). The F_{ST} distri-
482 bution calculated between the simulated A and B lineages, as the distribution obtained
483 with the real data, is indeed largely shifted towards low values (Figure 3b). These latter
484 results demonstrate that bottlenecks did not lead to elevated genetic differentiation
485 at the genome-wide level. As such, the high F_{ST} value we observed suggest that most
486 flowering-time genes are under selection.

487

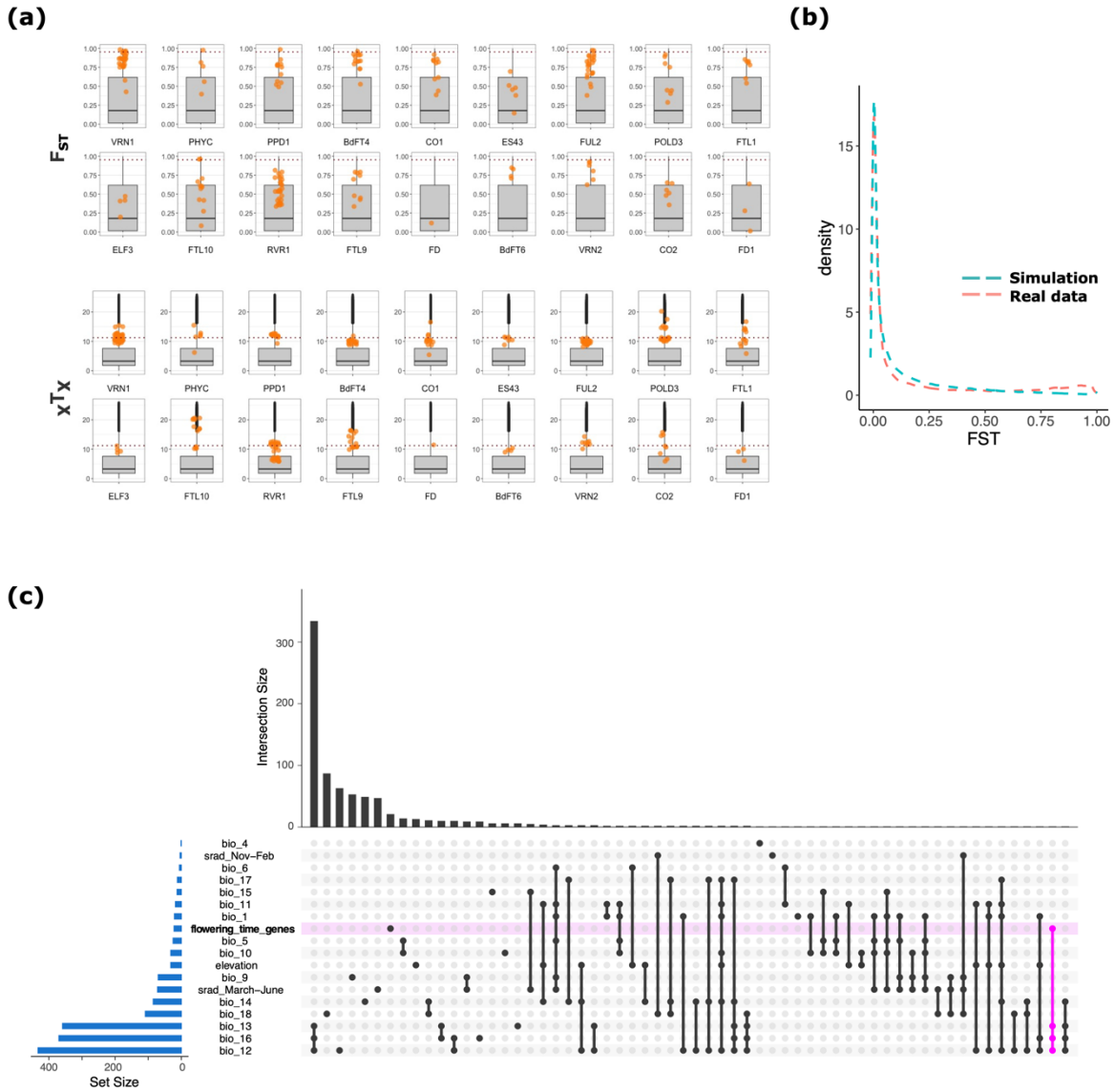

Fig. 3: Flowering-time gene differentiation (a) Top: Single SNP FST computed for the 56 accessions of the A and B lineages (dashed line = 5% outliers); bottom: single SNP XTX computed at the genetic clade level (dashed line = 1% POD threshold). (b) Distribution of FST calculated between the A and B lineage with real and forward-simulated data under a neutral scenario. (c) Upset plot displaying the overlap between gene sets identified with the GEAs performed by Minadakis et al. (2023) for 23 bioclimatic variables and flowering-time genes.

Genome-wide scans of positive selection

To properly test for positive selection while accounting for the structure and demographic history of our populations, we computed X^TX statistics, a measure comparable to single SNP F_{ST} that accounts for the neutral covariance structure across populations. In brief, we computed X^TX with our actual SNP dataset over the entire diversity panel

493 using the five genetic clades as focal populations. We then simulated a pseudo-ob-
494 served dataset (POD) of 100,000 SNPs under the demographic model inferred from
495 the covariance matrix of the actual SNP dataset. X^TX statistics were then computed for
496 the POD to determine the probability of neutrality for each SNP. The threshold of sig-
497 nificance was thus set to 11.2, a value slightly lower than the 1% outlier threshold
498 (13.6). Many flowering-time genes display SNPs more differentiated than expected un-
499 der a neutral scenario (Figure 3b) suggesting that those genes have evolved under
500 positive selection. Nine flowering-time genes *PHYTOCHROME C* (*PHYC*), *VRN1*, CON-
501 STANS 1 and 2 (*CO1* and *CO2*), *POLD3*, *FTL1*, *FTL10*, *FTL9* and *VRN2* display extremely
502 differentiated SNPs ($X^TX > 15$) both in the subset of accessions (Figure 3a) and in the
503 entire diversity panel (Figure S4c). We also tested for extended haplotypes and foot-
504 print of selective sweeps with the integrated Haplotype Score (iHS). However, none of
505 those highly flowering-time genes are located in regions displaying significantly longer
506 haplotypes (Figure S5).

507 We ran SnpEff to test which SNPs in flowering-time genes are more likely to have a
508 functional impact. Only few SNPs in *CO2*, *ES43*, and *Photoperiod-H1* (*PPD1*) were cat-
509 egorized as variants with high impact while the large majority of SNPs in other genes
510 were categorized as variants with moderate and low effect (Figure S6), rendering the
511 identification of the potential targets of selection challenging for most of our genes of
512 interest.

513 In order to characterize which environmental factors might have shaped diversity at
514 flowering-time genes, we eventually made use of genotype-environment association

515 (GEA) analyses performed by Minadakis et al. (2023) with bioclimatic variables associ-
516 ated to precipitation levels, temperature or elevation. We found that only one of the
517 22 flowering-time genes (Bradi2g59119, *ODDSOC2*-like) showed an overlap with the
518 gene sets significantly associated with current bioclimatic variables (Figure 3c).

519 Yet, the GEAs performed by Minadakis et al. corrected for population structure and
520 can hence result in false negative since the genetic clades occupy different ecological
521 niches. We indeed found significant associations between SNPs at flowering-time gene
522 and bioclimatic variables such as Bio14 (Precipitation of driest quarter) and aridity lev-
523 els in spring, when not accounting for population structure (Kendall correlation; Figure
524 S7a), indicating that the confounding effect of population structure and adaptation at
525 a regional scale may mask the significant effect of the environment on flowering-time
526 genes diversity.

527

528 **Potential adaptation to past climatic conditions**

529 We estimated the age of flowering-time alleles and found that those arose relatively
530 recently between 9,000 to 38,000 years ago (Table S7) as most alleles in our system
531 (Minadakis et al. 2023). We speculated that variation in flowering time could also re-
532 flect adaptation to recent past conditions, potentially to the last glacial maximum
533 (LGM) 22,000 years ago. We therefore tested whether the delay in flowering time we
534 observed in accessions from the A_East and A_Italia clades could result from an adap-
535 tation to past colder climates. To do so, we used the niche suitability projections under
536 LGM conditions computed by Minadakis et al (2023). We selected a set of 200 random

537 points per clade in highly suitable habitats and extracted the 19 LGM bioclimatic vari-
538 ables for the corresponding sites. The PCA performed with these 19 LGM bioclimatic
539 variables do not allow us to separate the five genetic clades. Altogether, accessions
540 from the A_East and A_Italia clades neither occurred in colder nor in wetter environ-
541 ments than the B_East, B_West and C accessions (Figure S8) which suggests that the
542 extended vernalization requirement and delay in flowering we observed for the A_East
543 and A_Italia accessions were not selected during LGM.

544

545

546 **Long-range linkage disequilibrium among flowering-time genes**

547 A striking pattern eventually emerges from the former analyses. The fact that the flow-
548 ering-time genes gave nearly identical signals with regard to their association with
549 flowering time suggests, as displayed in Figure 2b, that SNPs at flowering-time genes
550 harbor similar allele frequencies. These similar allele frequencies indicate that some
551 flowering-time genes might be co-selected (polygenic selection) and remain in strong
552 linkage disequilibrium despite the large physical distances that separate them (Zan
553 and Carlborg 2019; Gupta et al. 2023).

554 To formerly test this hypothesis, we computed LD among the 20 focal SNPs used
555 for the RDA analyses. LD computed among pairs of focal SNPs in the 56 selected ac-
556 cessions as well as in the entire diversity panel show a similar pattern: many flowering-
557 time genes display high LD despite the large distances that separate them on a given
558 chromosome (Figure 4b). This is especially true for flowering-time genes located on

559 chromosome 1 and 2 (Bd1 and Bd2), which are found in much higher LD than expected

560 considering the 95% confidence interval (CI) of the genome-wide LD-decay (Figure 4c).

561 Strikingly, we also found very high LD among flowering time-genes located on dif-

562 ferent chromosomes both in the selected accessions and entire diversity panel (Figure

563 4b). Located on chromosome 1, *VRN1* for instance, is in strong LD with eight other

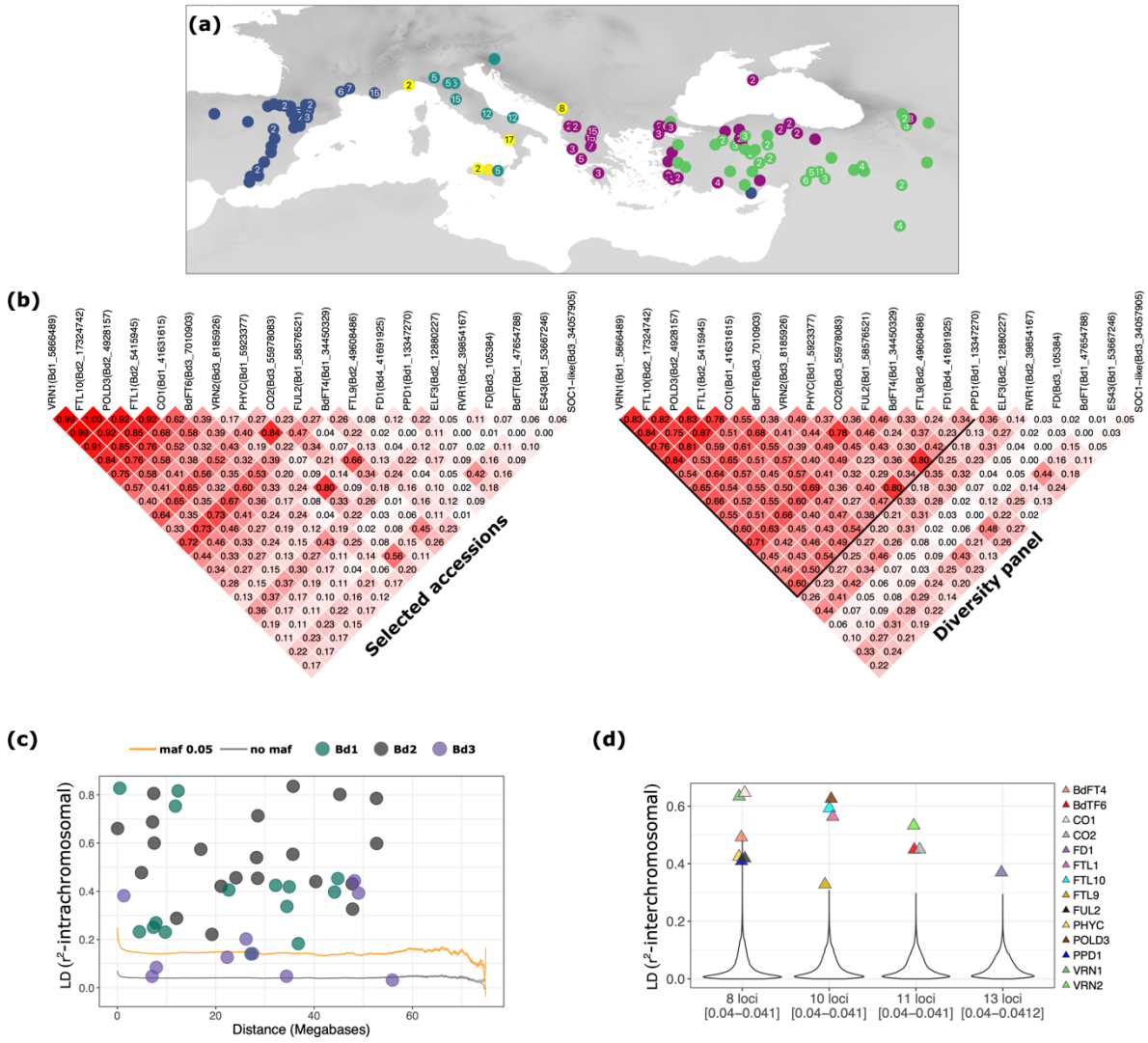

Fig.4 Linkage disequilibrium (LD) in the flowering time pathway a) Map displaying the locality of the 332 sequenced accessions composing the diversity panel b) LD among flowering-time genes in the selected accessions and diversity panel. For the diversity panel, the black lines delimit the focal genes used for the interchromosomal LD analysis. c) LD decay computed over the entire diversity panel. The orange and grey lines display the 95% CI of the LD decay calculated with or without filtering for a minimum allele frequency (maf) respectively. Dots display LD between pairs of flowering-time genes located on the same chromosome d) Distribution of LD among loci located on different chromosomes. The violin plots display the means of LD calculated among eight, ten, eleven and 13 loci. Numbers in square brackets indicate the confidence interval around the mean.

564 genes located on chromosome 2 (*POLD3*, LD = 0.84; *FTL9*, LD = 0.45, *FTL1*, LD = 0.76;
565 *FTL10*, LD = 0.83), chromosome 3 (*VRN2*, LD = 0.65; *CO2*, LD = 0.55, *BdFT6*, LD = 0.54)
566 and chromosome 4 (*BdFT4*, LD = 0.71). To test to what extent this long-range LD
567 among the 14 focal flowering-time genes deviates from genome-wide patterns, we
568 computed LD for a subset of 50,000 random pairs of genic loci located on different
569 chromosomes across the genome. This allowed us to estimate the average inter-chro-
570 mosomal LD among loci (Figure 4d). For each combination, the inter-chromosomal LD
571 we observed among eight loci (for focal flowering-time genes located on chromo-
572 somes 1), ten loci (for focal flowering-time genes located on chromosomes 2), eleven
573 loci (for focal flowering-time genes located on chromosomes) and 13 loci (for focal
574 flowering-time genes located on chromosomes 4) was largely outside the CI calculated
575 with random genic loci (Figure 4d).

576 Note that *FRUITFULL-like* (*FUL2*) and *PPD1* are the only genes displaying putative
577 footprint of insertion polymorphisms in the diversity panel (Table S5). Furthermore, in
578 a selfing species like *B. distachyon*, heterozygous SNPs are hallmarks of gene duplica-
579 tion (Jaegle et al. 2023; Stritt et al. 2022). Using a vcf file not filtered for heterozygous
580 SNPs, we found that only 0.6% of the SNPs located in flowering-time genes are heter-
581 ozygous across the 332 accessions. These results imply that flowering-time genes are
582 occurring in single copy and that structural rearrangements or duplications did not
583 alter their position in non-reference genomes. Taken together, these results indicate
584 that the long-range LD among flowering-time genes as well as their differentiation
585 levels deviate from genome-wide patterns and are difficult to explain by the

586 demographic history of the population alone. We hence conclude that 14 flowering-
587 time genes (Figure 4d) are co-evolving and undergo polygenic selection.
588

589 **Genome-wide association for flowering time variation measured in outdoor**
590 **conditions**

591 Greenhouse conditions are far from any natural optimum and may obscure association
592 with relevant environmental cues, while taking an environment closer to the natural
593 conditions encountered by of one or several clades acts as a useful pivot to contrast
594 clades. Hence, we eventually made use of flowering time data we collected for a subset
595 of 131 accessions (Stritt et al. 2022) in Zürich, Switzerland, to assess flowering time
596 variation in semi-natural conditions. While *B. distachyon* do not occur at such latitudes
597 (Minadakis et al. 2023), a PCA performed with the 22 bioclimatic variables on our 332
598 natural accessions and including a site in Zurich shows that the environmental
599 conditions in Zürich are not different from the ones encountered by ABR9 for instance
600 (Figure 5a, Table S2 for bioclimatic data). While other biotic (vegetation type and
601 density) and abiotic (soil characteristic) factors are certainly preventing the species
602 from occurring in northern latitude, Zürich harbours climatic conditions similar to ones
603 encountered by the species at the northern margin of its natural distribution, making
604 it a valid experimental site to study flowering time in *B. distachyon*.

605 In brief, we planted seeds for 131 accessions (Figure 5b) outdoors in November
606 2017, in the Botanical Garden of Zurich, Switzerland, with six replicates per accession
607 and recorded flowering time in spring. 31 of the accessions used in the greenhouse

experiment are used in the outdoor experiment, including four (Ren4, Lb1, Lb23 and Cm7) of the five accessions that did not flower by the end of the experiment. All plants flowered within 20 days in April (Figure 5c). Flowering time for plants from the B_East and C clades were not significantly different (Kruskal-Wallis test, P-value = 0.96) but those accessions flowered significantly faster than accessions from the other clades (Kruskal-Wallis test, all P-values < 0.01). Plants from the A_Italia and B_West flowered significantly later than plants from the other clades (Kruskal-Wallis test, all P-values < 0.02) but were not significantly different from each other (P-value = 0.06). As such, the data collected outdoor contrasts with the ones collected in the greenhouse.

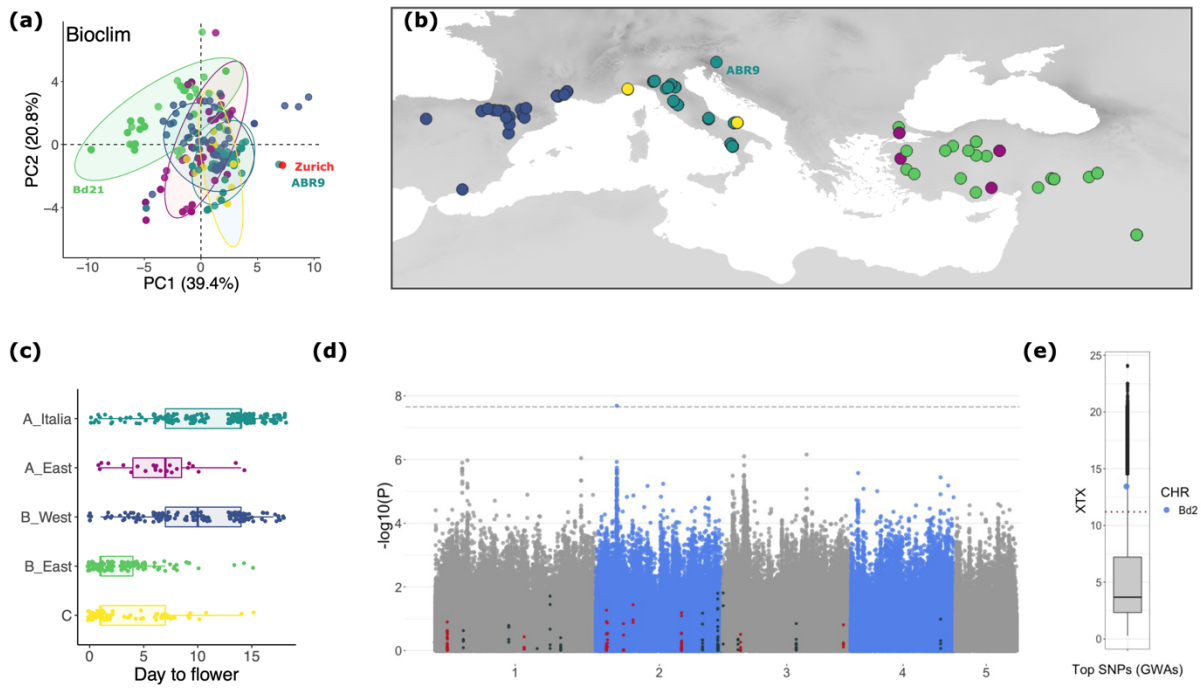

Fig. 5: Genome-wide association analysis with flowering time (outdoor experiment) a) PCA performed with 19 classical wordlclim variables combined to solar radiation in spring, global aridity in spring and altitude for the 332 accessions of the diversity panel and a locality in Zurich b) Geographical origin of the 131 accessions used for the experiment c) Flowering time per cluster (displaying replicates) d) Manhattan plot displaying the association between SNPs and flowering time. The red and dark dots display SNPs located into AFT- or other flowering-time genes respectively. The dashed line corresponds to FDR threshold of significance e) XTX values for the top GWAs SNP on chromosome 2 (Bd2).

617 As for the greenhouse experiment, we used RDA to fit models where flowering-time
618 was independently entered as a response variable while the cluster of origin
619 (model = cluster alone), the 22 environmental variables (model = all bioclimatic varia-
620 bles) or both the cluster of origin and the 22 bioclimatic variables (model = cluster +
621 all bioclimatic variables) were successively entered as explanatory variables. We com-
622 pared those full-models to empty models where flowering-time was explained by a
623 fixed intercept alone (Capblancq and Forester 2023). We found that a large part of the
624 variance in flowering-time is explained by bioclimatic variables linked to precipitation
625 levels in warm months whether the models did or did not include the cluster of origin
626 (e.g. bio18 and bio12; Table 1).

627 A genome-wide association analysis (GWAs) performed with GEMMA (Zhou and
628 Stephens 2012) on the 131 accessions and 2,266,225 filtered SNPs (Figure S9 for marker
629 density) identified one significant peak which does not overlap with any of the 22
630 flowering-time genes we studied above (Figure 5d). We also made use of the GEAs
631 performed by Minadakis et al. (2023) and found that the gene underlying the peak
632 (Bradi2g11490, a carbohydrate-binding-like gene) does not overlap with the gene sets
633 significantly associated with current bioclimatic variables. Yet, similarly to what we
634 found for the AFT-genes, we found significant associations (Figure S7b) between SNPs
635 at the GWAs peak and bioclimatic variables, especially with Bio14
636 (Precipitation_of_Driest_Month), when not taking into account population structure.
637 Consistent with selection by the environment, the top GWAs SNP constitutes also an
638 X^TX outlier (Figure 5e).

639 # Discussion

640 **Flowering time-related traits and adaptation to local climate**

641 Flowering time has been shown to play an important role in local adaptation across
642 many plant systems including crops (Izawa 2007; Anderson et al. 2012; Anderson, et
643 al. 2013; Ågren et al. 2017; Navarro et al. 2017; Wadgymar et al. 2017; Takou et al. 2019;
644 Qian et al. 2020; Yan et al. 2021). In *B. distachyon*, flowering time has been mainly
645 studied from a molecular viewpoint, clarifying the role of specific genes in sensing
646 environmental variation such as day-length and temperature (Ream et al. 2012;
647 Ruelens et al. 2013; Ream et al. 2014; Woods et al. 2014; Woods et al. 2017[a,b]; Lomax
648 et al. 2018; Cao et al. 2020; Kennedy and Geuten 2020; Woods et al. 2020; Bouché et
649 al. 2022; Raissig and Woods 2022). While those studies underline the complex archi-
650 tecture of flowering-time and revealed large variation regarding vernalization require-
651 ment among natural accessions for instance, they provide little information with regard
652 to adaptation.

653 In fact, the wide range of vernalization requirement observed in *B. distachyon*
654 suggests that local adaptation of flowering time could take place through distinct de-
655 velopmental thresholds (i.e the accumulated amount of 'developmental time' required
656 for a given developmental stage to allow a transition to the next developmental stage
657 see Donohue et al. 2014) among accessions. Indeed, in a widespread Mediterranean
658 species like *B. distachyon*, not all accessions are exposed to long and harsh winter (Fig-
659 ure S2). The expression of traits such as the minimum duration of vernalization neces-
660 sary to permit flowering might be contributing *in fine* to flowering time variation in

661 the wild and be especially relevant to investigate in the context of local adaption. We
662 indeed observed a significant albeit partial correlations among the four flowering time-
663 related traits we investigated (Figure 1b) indicating that these traits constitute different
664 components of flowering time.

665 Estimating the effect of the environment remains a challenge in such structured
666 populations. Yet, we show a significant association between flowering time-related
667 traits and bioclimatic variables in addition to the cluster effect, indicating that flower-
668 ing time-related traits are locally adapted trait in our system. Because bioclimatic var-
669 iables are largely correlated among each other's, pinpointing the selective constraints
670 acting on flowering time-related traits is equally difficult (Capblancq and Forester
671 2023). Our RDA analyses, however, point at bioclimatic variables which are biologically
672 meaningful as linked to aridity levels in warm months. As such, precipitation levels and
673 hence water limitation seem especially important for flowering time-related traits as
674 already shown for broader fitness effects in our species (Des Marais et al. 2017). In our
675 system, MTD and day to flower after MTD have never been investigated. It is therefore
676 very interesting to see that those two traits also display signs of local adaptation. Our
677 results therefore advocate for a complex adaptation of flowering time and suggest
678 that vernalization saturation might not be necessary in the wild to synchronize flower-
679 ing time with the environment.

680

681

682

683 **Early- and late-flowering genotypes are unlikely driven by adaptation**

684 The greenhouse experiment further confirms that *B. distachyon* natural accessions
685 vary greatly regarding their vernalization saturation requirement and ultimately flow-
686 ering time and can be broadly grouped into early- and late-flowering genotypes (Fig-
687 ure S1 and Figure 1, but see Ream et al., 2014; Gordon, et al. 2017 for a finer classifi-
688 cation scheme). Despite within clade variation regarding flowering time after vernali-
689 zation saturation (Figure 1c), accessions from the A lineage (A_East and A_Italia) display
690 a large delay in flowering compared to accessions from the B (B_East and B_West) and
691 C lineage, which typically result from longer vernalization saturation requirements. This
692 pattern has been suggested to be a sign of adaptation at a regional scale in Turkey
693 (Skalska et al. 2020) and could be interpreted as a footprint of diversifying selection at
694 the genetic clade level. Based on this hypothesis, accessions from the A_East and A_Ita-
695 lia clades may display a delay in flowering as globally adapted to colder and less arid
696 environmental conditions, as shown for instance in *A. thaliana* (Ågren and Schemske
697 2012). Yet, our results do not fully support this scenario, as we only find partial corre-
698 lations between the partitioning of the phenotypes and the bioclimatic variables asso-
699 ciated with flowering time (Figure 1 and Figure S3). Our niche modelling projections
700 for the last glacial maximum (Minadakis et al. 2023), do not further support an adap-
701 tation to the last glacial maximum conditions (Figure S8). As such, the partitioning of
702 the early vs. late flowering accessions remains difficult to explain with an "adaptive"
703 scenario. In summary, we conclude that local environmental conditions are partly

704 driving flowering time variation within genetic clades but not the early- and late-flow-
705 ering partitioning of the phenotypes we observed among clades in the greenhouse.

706 We have not tested different combinations of vernalization temperature and length.
707 In *A. thaliana* for instance, natural ecotypes have characteristic vernalization tempera-
708 ture profiles and vernalization temperature ranges from 0 to 14 °C (Duncan et al. 2015).
709 While *B. distachyon* does not occur in a wide range of latitude as *A. thaliana*, it is clear
710 that interactions between vernalization temperature and length are likely to play a role
711 as well. As already shown by Stritt et al. (2022) with a smaller subset of accessions,
712 variation in flowering time is for instance largely attenuated in outdoor conditions and
713 although significant differences are observed among genetic clades, all plants flowered
714 within 20 days when grown outdoors in Zürich (Figure 5c), including the four acces-
715 sions that did not flower with the greenhouse experiment. Hence, greenhouse experi-
716 ments, as largely performed in *B. distachyon* (Ream et al. 2014; Gordon, et al. 2017;
717 Sharma, et al. 2017) may only weakly capture how accessions behave in the wild.

718

719 **Flowering-time genes and flowering time-related traits**

720 We also selected 22 flowering-time genes known to play a major role in vernalization-
721 (e.g., *VRN1*, *POLD3*) or photoperiod-sensing (e.g. *PPD1*, *PHYC*) to characterize the
722 magnitude of their allelic effects on flowering time-related traits. We found that SNPs
723 in those 22 genes display relatively large association with the number of days to flower
724 after vernalization saturation and to some extent with MTD or vernalization saturation

725 but only poorly with the number of days to flower after MTD (Figure 2a). Interestingly,
726 genes known to play a role in cold-mediated vernalization such as *VRN1* or *POLD3*
727 (Raissig and Woods 2022) show a larger association with MTD than with vernalization
728 saturation, suggesting that those genes are important for cold perception regardless
729 of its length.

730 Here again, our RDA analyses show that disentangling the effect of the cluster of
731 origin from the one of single SNPs is challenging. We indeed observed a strong parti-
732 tioning of the reference and alternative alleles in flowering-time genes among genetic
733 clades and lineages (Figure 2b). The high genetic differentiation of flowering-time
734 genes between the A and B lineages (Figure 2b) could result from the recent bottle-
735 necks experienced by *B. distachyon* in the recent past (Stritt et al. 2018; Minadakis et
736 al. 2023) and produce spurious association with flowering-time related traits. Three
737 lines of evidence rule out this demographic scenario.

738 First, our 22 candidate genes have been shown to play an important role in photo-
739 period sensing, vernalization and *in fine* in flowering variation among diverse *B. dis-*
740 *tachyon* accessions not only by sequence homolgy but also via molecular, biochemical,
741 and genetic methods (Wu et al. 2013; Ream et al. 2014, Woods et al. 2014, Woods et
742 al. 2017[a] , Woods et al. 2017[b] , Lomax et al. 2018; Qin et al. 2019, Woods et al. 2019,
743 Woods et al. 2020, Raissig and Woods 2022, Bouché et al. 2022; Alvarez et al. 2023;
744 Woods et al. 2023). It is therefore legitimate to assume that they might play a role in
745 regulating flowering time-related traits in genetically diverse accessions as well.

746 Second, FST analyses performed with our real- as well as forward-simulated data
747 show that the population size reduction experienced by *B. distachyon* did not lead to
748 genome-wide highly differentiated alleles and SNPs at flowering-time gene constitute
749 clear FST outliers. The X^TX analysis we performed with the five genetic clades as focal
750 populations also shows that most of the flowering-time genes harbor SNPs above the
751 threshold of significance, *POLD3* and *CO1* presenting more extreme outliers. This foot-
752 print of positive selection (Gautier 2015) is yet not accompanied by extended haplo-
753 types around our candidate genes (except for *CO2*) which implies that the initial selec-
754 tive sweeps may have eroded with time and that selection did not occur in a recent
755 past. Flowering-time gene are yet not colocalizing with regions we previously identi-
756 fied with GEA analyses (Figure 3c). Thus, although we find evidence of positive selec-
757 tion at single flowering-time genes, the selective constraint at play remains yet to be
758 identified. It is yet essential to keep in mind that GEA performed in species with strong
759 population structure can lead to high rate of false negatives as they typically include
760 structure correction (Lottheros 2023; Booker et al. 2023). We did find significant asso-
761 ciations between bioclimatic variables and SNPs at flowering-time genes when not
762 correcting for population structure (Figure S6). Common garden experiments will thus
763 be key to test the effect of genotype-by-environment interactions in our system.

764 Third, we highlighted a striking pattern of long-range linkage disequilibrium (LD),
765 both intra- and inter-chromosomal, among 14 flowering-time genes associated with
766 flowering time variation under greenhouse conditions (Figure 4). Polygenic selection
767 is expected to result in LD between regions under selection (Gupta et al. 2023; Yeaman

768 et al. 2016; 2018) but only few cases have been reported so far in plants and animals
769 (Hohenlohe et al. 2012; Yeaman et al. 2016; Gupta et al. 2023; Park 2019). In *A. thali-*
770 *ana,* Zan and Carlborg (2019) also identified long-range LD among four clusters of
771 flowering-time genes. We demonstrated that the levels of long-range LD (intra- and
772 inter-chromosomal) we observed among 14 flowering-time genes (Figure 4) are not
773 observed among random genic loci in the genome. As flowering-time genes do not
774 display signs of duplication or insertion polymorphisms, we imply that structural rear-
775 rangements did not bring flowering-time gene physically together in non-reference
776 accessions. We therefore believe that we present clear evidence for polygenic selection
777 on key genes involved in the flowering pathway. Expression analyses further support
778 the functional connection among these loci in *B. distachyon* and grasses in general.
779 For example, *VRN1* and *FTL1* are expressed in a positive feedback loop, which over-
780 comes the flowering repression of *VRN2* (Ream et al. 2014; Woods et al. 2016; Woods
781 et al. 2017[b]). Additionally, there is an intricate connection between many of these flow-
782 ering-time genes both transcriptionally and at the protein level. For example, among
783 the pairwise interactions tested between *PHYC*, *PHYB*, *ELF3*, *PPD1*, *VRN2*, *CO1*, and
784 *CO2* more than 80% showed positive interactions in yeast two hybrid assays some of
785 which have been verified *in planta* (Shaw et al. 2020; Alvarez et al. 2023). Thus, many
786 flowering-time genes in LD can interact at multiple levels.

787 Altogether, this set of analyses show that the association between flowering-time
788 genes and flowering time-related traits, especially days to flower after vernalization
789 saturation, is a result of selection and unlikely due to population structure.

790 Interestingly, while *pold3* and *elf3* loss of function mutants flower faster than the
791 wildtype (Bouché et al. 2022;. Woods et al. 2020), their contribution to flowering time
792 after vernalization saturation for instance (39% and 15% respectively) differ drastically.
793 This discrepancy might be due to the fact that mutants used to characterize gene func-
794 tions usually harbor mutations with deleterious or large effect size (loss of function).
795 In contrast, our natural flowering-time gene variants are mostly predicted as having
796 low to moderate suggesting that they modulate flowering time-related traits quanti-
797 tatively. As such, one should remain cautious while extrapolating the effect of flower-
798 ing-time variants from mutant-based experiments.

799

800 **GWAs detect additional candidate genes for flowering time**

801 None of the flowering-time genes co-localize with the GWAs candidate identified
802 with the outdoor experiment (Figure 5d). It is clear that the partitioning of the refer-
803 ence and alternative variants at flowering-time genes (Figure 2a) largely dimmish our
804 detection power as we applied a correction for population structure. Yet, while we
805 should extend our common garden experiment to a larger number of sites, our results
806 are in line with a previous studies in *A. thaliana* which, by using natural accessions and
807 RILs, found that flowering time variation scored in the field experiment poorly corre-
808 lated with the flowering time variation obtained under greenhouse conditions (Wilczek
809 et al. 2010; Brachi et al. 2010; Malmberg et al. 2005; Weinig et al. 2002). As a conse-
810 quence, a limited overlap is observed between the genomic regions detected in field
811 experiments and those detected under greenhouse conditions (Brachi et al. 2010).

812 Flowering time has a complex polygenic architecture (Buckler 2009; Brachi et al. 2010;
813 Navarro et al. 2017; Zan and Carlborg 2019; Gaudinier and Blackman 2020) and the
814 use of EMS-induced mutants suggested that many additional genes might play a role
815 in shaping this trait in *B. distachyon* (Raissig and Woods 2022), some of which are not
816 described or only play a minor role in flowering time in other plant models (Woods et
817 al. 2020). In addition, alleles may affect phenotypes only in specific populations (Yan
818 et al. 2021; Gloss et al. 2022; Zan and Carlborg 2019) or seasons (Weinig et al. 2002;
819 Gould and Stinchcombe 2017). Taking into account the polygenic architecture, gene-
820 by-environment association and phenotypic plasticity (Gaudinier and Blackman 2020;
821 Yan et al. 2021) will therefore be essential to better capture the adaptive potential of
822 flowering time and flowering-time genes in natural populations of *B. distachyon.* Alt-
823 hough flowering-time genes are undoubtedly essential in the perception of environ-
824 mental cues and overwintering (for review Raissig and Woods 2022), our results show
825 that the effect of their variants in the wild are more difficult to predict and that addi-
826 tional genes may be at play.

827

828 **Conclusion and perspectives**

829 Our results suggest that i) flowering time-related traits are a locally adapted trait in
830 *B. distachyon* but ii) part of the variation in those traits can be explained by the
831 environment and by SNPs in key flowering-time genes and, iii) key flowering-time
832 genes are co-evolving but their effect in the wild remains to be clarified. In the face of
833 global warming, plant phenology has recently advanced significantly (e.g. Anderson et

834 al. 2012). Investigating the polygenetic architecture of flowering time therefore
835 remains a timely question. Polygenic selection, epistatic and pleiotropic effects might
836 limit the evolution of traits (Yan et al. 2021; Yeaman 2022) and future experiments in
837 *B. distachyon* should focus on disentangling these effects. Mimicking the combination
838 of the various clues that trigger flowering is yet impractical under greenhouse
839 conditions and common garden experiments will thus be essential to place flowering
840 time in a natural context in this system. We, however, know relatively little about the
841 basic ecology of *B. distachyon*. Fundamental questions now need to be addressed to
842 more broadly characterize the process of local adaptation in this species. These
843 include: when are plants emerging in the wild?; how plastic are flowering time and
844 phenotypes in general?; and what is the contribution of seed banks to the effective
845 population size and hence selection strength? Answering these will undoubtedly
846 represent remarkable progress in our understanding of *B. distachyon's* ecology.
847
848

849 Author contribution

850 NM conceived the study, performed the greenhouse experiment, contributed to the
851 analysis and the writing of the manuscript. MT collected samples, contributed to the
852 analysis. WX, RH and LK contributed to the analysis. DPW contributed with the writing
853 of the manuscript. ACR conceived the study, contributed to the analysis and with the
854 writing of the manuscript.

Data availability

Seeds will be distributed through GRIN (https://www.ars-grin.gov). Accession numbers for sequencing data can be found in (Gordon et al. 2017; Gordon et al. 2020; Skalska et al. 2020; Stritt et al. 2022; Minadakis et al. 2023). The raw data of the flowering time measurements are available in the supplementary materials. Bioclimatic variable can be downloaded at https://www.worldclim.org/data/bioclim.html and extracted using the R code "download_worldclim2.1.R" provided by Minadakis et al. 2023 (https://zenodo.org/records/8354318). RDA analyses were adapted from the detailed scripts provided by Capblancq and Forester (2023; https://github.com/Capblancq/RDA-landscape-genomics/tree/main)

Acknowledgments

We would like to thank the Swiss National Science foundation (project 31003A_182785) and the Research Priority Program Evolution in action from the University of Zurich for their generous funding. The authors are grateful to Beat Keller and Ueli Grossniklaus for providing space for the flowering time experiments as well as the Amasino lab, Sam Yeaman and Dieter Ebert for stimulating discussion on flowering time and polygenic selection. We eventually would like to thank the two anonymous reviewers for their time and very constructive comments.

876 # Supplementary Materials

877 The supplementary materials consist in nine figures (File Supplementary figures) and
878 seven tables.

879 **Table S1: Raw results of the flowering time experiment.**

880 **Table S2: Bioclimatic variable extracted for the 332 accessions of the diversity panel**

881 **Table S3: Flowering time-related traits extracted from the greenhouse experiment**

882 **Table S4: Differences in flowering time-related traits among the five genetic clades.**

883 **Table S5: Flowering time gene position and ID.**

884 **Table S6: RDA output for the four flowering time-related traits again the 502 SNPs.**

885 **Table S7: Flowering-time gene age estimates.**

886

887 # References

888 Ågren J, Oakley CG, Lundemo S, Schemske DW. 2017. Adaptive divergence in flowering
889 time among natural populations of Arabidopsis thaliana: Estimates of selection and
890 QTL mapping. Evolution. 71:550–564.

891 Ågren J, Schemske DW. 2012. Reciprocal transplants demonstrate strong adaptive
892 differentiation of the model organism Arabidopsis thaliana in its native range. New
893 Phytol. 194:1112–1122.

894 Albers PK, McVean G. 2020. Dating genomic variants and shared ancestry in
895 population-scale sequencing data. PLoS Biol. 18:1–26.

896 Alvarez MA, Li C, Lin H, Joe A, Padilla M, Woods DP, Dubcovsky J. 2023. EARLY
897 FLOWERING 3 interactions with *PHYTOCHROME B* and *PHOTOPERIOD1* are critical
898 for the photoperiodic regulation of wheat heading time. PLOS Genet. 19(5):
899 e1010655.

900 Anderson JT, Inouye DW, McKinney AM, Colautti RI, Mitchell-Olds T. 2012. Phenotypic
901 plasticity and adaptive evolution contribute to advancing flowering phenology in
902 response to climate change. Proc. R. Soc. B Biol. Sci. 279:3843–3852.

903 Anderson JT, Lee CR, Rushworth C, Colautti R and Mitchell-Olds T. 2013. Genetic
904 tradeoffs and conditional neutrality contribute to local adaptation. Mol Ecol 22:699–
905 708.

906 Andrés F, Coupland G. 2012. The genetic basis of flowering responses to seasonal cues.
907 Nature Reviews Genetics. 13, 627–639.

908 Bettgenhaeuser J, Corke FMK, Opanowicz M, Green P, Hernández-Pinzón I, Doonan JH,
909 Moscou MJ. 2017. Natural variation in brachypodium links vernalization and
910 flowering time loci as major flowering determinants. Plant Physiol. 173:256–268.

911 Blackman BK. 2017. Changing responses to changing seasons: Natural variation in the
912 plasticity of flowering time. Plant Physiol. 173:16–26.

913 Blümel M, Dally N, Jung C. 2015. Flowering time regulation in crops-what did we learn
914 from Arabidopsis? Curr. Opin. Biotechnol. 32:121–129.

915 Booker TR, Yeaman S, Whiting JR, Whitlock MC. 2023. The WZA : A window-based
916 method for characterizing genotype–environment associations. Mol. Ecol.
917 Resour.00 : 1–16.

918 Borcard D, Gillet F, Legendre P. (2018). Numerical ecology with R (2nd ed.). Springer
919 International Publishing AG, part of Springer. https://doi.org/10.1007/978-3-319-
920 71404-2

921 Bouché F, Woods DP, Linden J, Li W, Mayer KS, Amasino RM, Périlleux C. 2022. EARLY
922 FLOWERING 3 and Photoperiod Sensing in Brachypodium distachyon. Front. Plant
923 Sci. 12:1–14.

924 Bourgeois Y, Stritt C, Walser JC, Gordon SP, Vogel JP, Roulin AC. 2018. Genome-wide
925 scans of selection highlight the impact of biotic and abiotic constraints in natural
926 populations of the model grass Brachypodium distachyon. Plant J. 96:438–451.

927 Brachi B, Faure N, Horton M, Flahauw E, Vazquez A, Nordborg M, Bergelson J, Cuguen
928 J, Roux F. 2010. Linkage and association mapping of Arabidopsis thaliana flowering
929 time in nature. PLoS Genet. 6:40.

930 Buckler ES et al. 2009. The Genetic Architecture of Maize. 325:714.

931 Cao S, Luo X, Xie L, Gao C, Wang D, Holt BF, Lin H, Chu C, Xia X. 2020. The florigen
932 interactor BdES43 represses flowering in the model temperate grass Brachypodium
933 distachyon. Plant J. 102:262–275.

934 Capblancq T and Forester B. 2023. Redundancy analysis: A Swiss Army Knife for land-
935 scape genomics. Methods Ecol Evol. 2021;12:2298–2309.

936 Cingolani P , Platts A, Wang L, Coon M, Nguyen T, Wang L, Land SJ, Lu X, Ruden DM.
937 2012. A program for annotating and predicting the effects of single nucleotide
938 polymorphisms, SnpEff: SNPs in the genome of Drosophila melanogaster strain. Fly
939 6:80-92.

940 Chouard P. 1960. Vernalization and its Relations to Dormancy. Annu. Rev. Plant Physiol.
941 11:191–238.

942 Danecek P, Auton A, Abecasis G, Albers CA, Banks E, Depristo MA, Handsaker RE, Lunter
943 G, Marth GT, Sherry ST, et al. 2011. The variant call format and VCFtools.
944 Bioinformatics 27:2156–2158.

945 Del'Acqua MD, Zuccolo A, Tuna M, Gianfranceschi L, Pè ME. 2014. Targeting
946 environmental adaptation in the monocot model Brachypodium distachyon : a
947 multi-faceted approach. BMC Genomics15:801.

948 Duncan S, Holm S, Questa J, Irwin J, Grant A, Dean C. 2015. Seasonal shift in timing of
949 vernalization as an adaptation to extreme winter. eLife e06620.

950 Eichten S, Stuart T, Srivastava A, Borevitz J. 2016. DNA Methylation profiles of diverse
951 Brachypodium distachyon aligns with underlying genetic diversity. Genome Res.
952 26(11):1520-1531.

953 Gaudinier A, Blackman Benjamin K. 2020. Evolutionary processes from the perspective
954 of flowering time diversity. New Phytol. 225:1883–1898.

955 Gautier M. 2015. Genome-Wide Scan for Adaptive Divergence and Association with
956 Population-Specific Covariates. Genetics 201(4):1555-79.

957 Gautier M, Vitalis R (2012). rehh: An R package to detect footprints of selection in
958 genome-wide SNP data from haplotype structure. Bioinformatics, 28(8) 1176-1177.

959 Gehlenborg N. 2019. UpSetR: A More Scalable Alternative to Venn and Euler Diagrams
960 for Visualizing Intersecting Sets. R package version 1.4.0. https://CRAN.R-pro-
961 ject.org/package=UpSetR.

962 Gloss AD, Vergnol A, Morton TC, Laurin PJ, Roux F, Bergelson J. 2022. Genome-wide
963 association mapping within a local Arabidopsis thaliana population more fully
964 reveals the genetic architecture for defensive metabolite diversity. Philos. Trans. R.
965 Soc. B Biol. Sci. 377: 20200512.

966 Gordon SP, Contreras-Moreira B, Levy JJ, Djamei A, Czedik-Eysenberg A, Tartaglio VS,
967 Session A, Martin J, Cartwright A, Katz A, et al. 2020. Gradual polyploid genome
968 evolution revealed by pan-genomic analysis of Brachypodium hybridum and its
969 diploid progenitors. Nat. Commun. 11:1–16.

970 Gordon SP, Contreras-moreira B, Woods DP, Marais DL Des, Burgess D, Shu S, Stritt C,
971 Roulin AC, Schackwitz W, Tyler L, et al. 2017. Extensive gene content variation in the
972 Brachypodium distachyon pan-genome correlates with population structure. Nat.
973 Commun. 8:2184.

974 Gould BA, Stinchcombe JR. 2017. Population genomic scans suggest novel genes
975 underlie convergent flowering time evolution in the introduced range of
976 Arabidopsis thaliana. Mol. Ecol. 26:92–106.

977 Gupta S, Harkess A, Soble A, Etten M Van, Leebens-Mack J, Baucom RS. 2023. Inter-
978 chromosomal linkage disequilibrium and linked fitness cost loci associated with
979 selection for herbicide resistance. New Phytol. 238:1263-1277.

980 Hall, Willis, Hall MC, Willis JH. 2006. Divergent selection on flowering time contributes
981 to local adaptation in Mimulus guttatuspopulations. Evolution. 60:2466–2477.

982 Haller BC, Messer PW. 2019. SLIM 3: forward genetic simulations beyond the Wright–
983 Fisher model. Molecular Biology and Evolution 36: 632–637.

984 Hasterok R, Catalan P, Hazen SP, Roulin AC, Vogel JP, Wang K, Mur LAJ. 2022.
985 Brachypodium: 20 years as a grass biology model system; the way forward? Trends
986 Plant Sci. 27:1002–1016.

987 Higgins JA, Bailey PC, Laurie DA. 2010. Comparative genomics of flowering time
988 pathways using *Brachypodium distachyon* as a model for the temperate Grasses.
989 PLoS One. 5(4): e10065.

990 Hijmans RJ, Van Etten J. (2012) Geographic analysis and modeling with raster data.
991 http://raster.r-forge.r-project.org/

992 Hohenlohe PA, Bassham S, Currey M, Cresko WA. 2012. Extensive linkage
993 disequilibrium and parallel adaptive divergence across threespine stickleback
994 genomes. Philos. Trans. R. Soc. B Biol. Sci. 367:395–408.

995 Huo N, Garvin DF, You FM, Luo SMM, Gu YQ, Lazo GR, Philip J. 2011. Comparison of a
996 high-density genetic linkage map to genome features in the model grass
997 Brachypodium distachyon. Theor. Appl. Genet. 123:455–464.

998 International Brachypodium Initiative. 2010. Genome sequencing and analysis of the
999 model grass {B}rachypodium distachyon. Nature 463:763–768.

1000 Izawa T. 2007. Adaptation of flowering-time by natural and artificial selection in
1001 Arabidopsis and rice. J. Exp. Bot. 58:3091–3097.

1002 Jaegle B, Pisupati R, Soto-Jiménez LM, Burns R, Rabanal FA, Nordborg M. 2023.
1003 Extensive sequence duplication in Arabidopsis revealed by pseudo-heterozygosity.
1004 Genome Biol. 24:1–19.

1005 Keitt TH, Bivand R, Pebesma E, Rowlingson B. 2010. RGDAL: bindings for the
1006 'Geospatial' data abstraction library. R package v.1.5-27. https://cran.r-
1007 project.org/web/packages/rgdal/index.html

1008 Kennedy A, Geuten K. 2020. The Role of FLOWERING LOCUS C Relatives in Cereals.
1009 Front. Plant Sci. 11:617340.

1010 Lomax A, Woods DP, Dong Y, Bouché F, Rong Y, Mayer KS, Zhong X, Amasino RM.
1011 2018. An ortholog of CURLY LEAF/ENHANCER OF ZESTE like-1 is required for proper
1012 flowering in Brachypodium distachyon. Plant J. 93:871–882.

1013 Lottheros K. 2023. The paradox of adaptive trait clines with nonclinal patterns in the
1014 underlying genes. Proc. Natl. Acad. Sci. 120: e2220313120

1015 Malmberg RL, Held S, Waits A, Mauricio R. 2005. Epistasis for fitness-related
1016 quantitative traits in Arabidopsis thaliana grown in the field and in the greenhouse.
1017 Genetics 171:2013–2027.

1018 Des Marais DL, Lasky JR, Verslues PE, Chang TZ, Juenger TE. 2017. Interactive effects of
1019 water limitation and elevated temperature on the physiology, development and
1020 fitness of diverse accessions of Brachypodium distachyon. New Phytol. 214:132–144.

1021 Minadakis N, Williams H, Horvath R, Stritt C, Thieme M, Bourgeois Y, Roulin AC. 2023.
1022 New resources for environmental genomics in the wild Mediterranean grass
1023 *Brachypodium. distachyon*. bioRxiv https://doi.org/10.1101/2023.06.01.543285

1024 Monnahan PJ, Kelly JK. 2017. The genomic architecture of flowering time varies across
1025 space and time in mimulus guttatus. Genetics 206:1621–1635.

1026 Nakagawa S, Schielzeth H. 2013. A general and simple method for obtaining R2 from
1027 generalized linear mixed-effects models. Methods Ecol. Evol. 4:133–142.

1028 Navarro JAR, Wilcox M, Burgueño J, Romay C, Swarts K, Trachsel S, Preciado E, Terron
1029 A, Delgado HV, Vidal V, et al. 2017. A study of allelic diversity underlying flowering-
1030 time adaptation in maize landraces. Nature genetics 49: 476–480.

1031 Nunes TDG, Zhang D, Raissig MT. 2020. Form, development and function of grass
1032 stomata. Plant J. 101:780–799.

1033 Nunes TDG, Berg LS, Slawinska MW, Zhang D, Redt L, Sibout R, Vogel J, Laudencia-
1034 Chingcuanco D, Jesenofsky B, Lindner H, Raissig MT. 2023. Regulation of hair cell
1035 and stomatal size by a hair cell-specific peroxidase in the grass *Brachypodium*
1036 *distachyon*. Curr. Biol. 33, 1844–1854.

1037 Oksanen J, Simpson JL, Guillaume F et al. (2022). vegan: Community Ecology Package.
1038 R package version 2.6-4. https://CRAN.R-project.org/package=vegan

1039 Park L. 2019. Population-specific long-range linkage disequilibrium in the human
1040 genome and its influence on identifying common disease variants. Sci. Rep. 9:1–13.

1041 Perdry H, Dandine-Roulland C (2022). gaston: Genetic Data Handling (QC, GRM, LD,
1042 PCA) & Linear Mixed Models. R package version 1.5.9. https://CRAN.R-
1043 project.org/package=gaston.

1044 Purcell S, Neale B, Todd-Brown K, Thomas L, Ferreira MAR, Bender D, Maller J, Sklar P,
1045 De Bakker PIW, Daly MJ, et al. 2007. PLINK: A tool set for whole-genome association
1046 and population-based linkage analyses. Am. J. Hum. Genet. 81:559–575.

1047 Qian C, Yan X, Shi Y, Yin H, Chang Y, Chen J, Ingvarsson PK, Nevo E, Ma XF. 2020.
1048 Adaptive signals of flowering time pathways in wild barley from Israel over 28
1049 generations. Heredity 124:62–76.

1050 Qin Z, Bai Y, Muhammad S, Wu X, Deng P, Wu J, An H, Wu L. 2019. Divergent roles of
1051 FT-like 9 in flowering transition under different day lengths in *Brachypodium*
1052 *distachyon*. Nat. Commun. 10:812

1053 Raissig MT, Woods DP. 2022. The wild grass Brachypodium distachyon as a
1054 developmental model system. Current Topics in Developmental Biology 147:33-71

1055 Ream TS, Woods DP, Amasino RM. 2012. The molecular basis of vernalization in
1056 different plant groups. Cold Spring Harb. Symp. Quant. Biol. 77:105–115.

1057 Ream TS, Woods DP, Schwartz CJ, Sanabria CP, Mahoy JA, Walters EM, Kaeppler HF,
1058 Amasino RM. 2014. Interaction of Photoperiod and Vernalization Determines
1059 Flowering Time of *Brachypodium distachyon*. Plant Physiol. 164:694–709.

1060 Ruelens P, Maagd RA, Proost S, Teissen G, Geuten K, Kaufmann K. 2013. FLOWERING
1061 LOCUS C in monocots and the tandem origin of angiosperm-specific. Nature Com.
1062 4:2280

1063 Sharma N, Ruelens P, D'hauw M, Maggen T, Dochy N, Torfs S, Kaufmann K, Rohde A,
1064 Geuten K. 2017. A flowering locus C homolog is a vernalization-regulated repressor
1065 in *Brachypodium* and is cold regulated in wheat. Plant Physiol. 173:1301–1315.

1066 Shaw LM, Li C , Woods DP, Alvarez MA, Lin H, Lau MY, Chen A, Dubcovsky J. 2020.
1067 Epistatic interactions between modulate the photoperiodic response in wheat. PLoS
1068 Genet 16(7): e1008812.

1069 Skalska A, Stritt C, Wyler M, Williams HW, Vickers M, Han J, Tuna M, Tuna GS, Susek K,
1070 Swain M, et al. 2020. Genetic and methylome variation in Turkish brachypodium
1071 distachyon accessions differentiate two geographically distinct subpopulations. Int.
1072 J. Mol. Sci. 21:1–17.

1073 Stritt C, Gimmi EL, Wyler M, Bakali AH, Skalska A, Hasterok R, Mur LAJ, Pecchioni N,
1074 Roulin AC. 2022. Migration without interbreeding: Evolutionary history of a highly
1075 selfing Mediterranean grass inferred from whole genomes. Mol. Ecol. 31:70–85.

1076 Stritt C, Gordon SP, Wicker T, Vogel JP, Roulin AC. 2018. Recent activity in expanding
1077 populations and purifying selection have shaped transposable element landscapes
1078 across natural accessions of themediterranean grass brachypodium distachyon.
1079 Genome Biol. Evol. 10:304–318.

1080 Stritt C, Thieme O, Roulin A.C. 2021. Detecting signatures of TE polymorphisms in
1081 short-read sequencing data. Methods Mol Biol. 2250:177-187.

1082 Stritt C, Wyler M, Gimmi EL, Pippel M, Roulin AC. 2020. Diversity, dynamics and effects
1083 of long terminal repeat retrotransposons in the model grass {B}rachypodium
1084 distachyon. New Phytol. 227:1736–1748.

1085 Takou M, Wieters B, Kopriva S, Coupland G, Linstädter A, De Meaux J. 2019. Linking
1086 genes with ecological strategies in Arabidopsis thaliana. J. Exp. Bot. 70:1141–1151.

1087 Wadgymar SM, Lowry DB, Gould BA, Byron CN, Mactavish RM, Anderson JT. 2017.
1088 Identifying targets and agents of selection: innovative methods to evaluate the
1089 processes that contribute to local adaptation. Methods Ecol. Evol. 8:738–749.

1090 Weinig C, Ungerer MC, Dorn LA, Kane NC, Toyonaga Y, Halldorsdottir SS, Mackay TFC,
1091 Purugganan MD, Schmitt J. 2002. Novel loci control variation in reproductive timing
1092 in Arabidopsis thaliana in natural environments. Genetics 162:1875–1884.

1093 Wickham H. 2016. ggplot2: Elegant Graphics for Data Analysis. Available from:
1094 https://ggplot2.tidyverse.org

1095 Wilczek AM, Burghardt LT, Cobb AR, Cooper MD, Welch SM, Schmitt J. 2010. Genetic
1096 and physiological bases for phenological responses to current and predicted
1097 climates. Philos. Trans. R. Soc. B Biol. Sci. 365:3129–3147.

1098 Wilhelm EP, Turner AS, Laurie DA. 2009. Photoperiod insensitive Ppd-A1a mutations in
1099 tetraploid wheat (Triticum durum Desf .). Theor. Appl Genet 118:285–294.

1100 Wilson PB, Streich JC, Murray KD, Eichten SR, Cheng R, Aitken NC, Spokas K,
1101 Warthmann N, Gordon SP, Vogel JP, et al. 2019. Global diversity of the
1102 Brachypodium species complex as a resource for genome-wide association studies
1103 demonstrated for agronomic traits in response to climate. Genetics 211:317–331.

1104 Woods DP, Li W, Sibout R, Shao M, Laudencia-Chingcuanco, Vogel J, Dubcovsky J,
1105 Amasino RM. 2023. PHYTOCHROME C regulation of photoperiodic flowering via
1106 PHOTOPERIOD1 is mediated by EARLY FLOWERING 3 in *Brachypodium distachyon*.
1107 PLoS Genet 19(5): e1010706.

1108 Woods D, Dong Y, Bouche F, Bednarek R, Rowe M, Ream T, Amasino R. 2019. A florigen
1109 paralog is required for short-day vernalization in a pooid grass. Elife 8:1–16.

1110 Woods DP, Bednarek R, Bouché F, Gordon SP, Vogel JP, Garvin DF, Amasino RM. 2017a.
1111 Genetic architecture of flowering-time variation in *Brachypodium distachyon*. Plant
1112 Physiol. 173:269–279.

1113 Woods DP, Dong Y, Bouché F, Mayer K, Varner L, Ream TS, Thrower N, Wilkerson C,
1114 Cartwright A, Sibout R, et al. 2020. Mutations in the predicted DNA polymerase
1115 subunit POLD3 result in more rapid flowering of *Brachypodium distachyon* . New
1116 Phytol. 227: 1725–1735

1117 Woods DP, McKeown MA, Dong Y, Preston JC, Amasino RM. 2016. Evolution of
1118 VRN2/Ghd7-like genes in vernalization-mediated repression of grass flowering.
1119 Plant Physiol. 170:2124–2135.

1120 Woods DP, Ream TS, Bouché F, Lee J, Thrower N, Wilkerson C, Amasino RM. 2017b.
1121 Establishment of a vernalization requirement in *Brachypodium distachyon* requires
1122 *REPRESSOR OF VERNALIZATION1*. Proc. Natl. Acad. Sci. 114:6623–6628.

1123 Woods DP, Ream TS, Minevich G, Hobert O, Amasino RM. 2014. PHYTOCHROME C is
1124 an essential light receptor for photoperiodic flowering in the temperate grass,
1125 Brachypodium distachyon. Genetics 198:397–408.

1126 Wu L, Liu Dongfeng, Wu J, Zhang R, Qin Z, Liu Danmei, Li A, Fu D, Zhai W, Mao L. 2013.
1127 Regulation of FLOWERING LOCUS T by a MicroRNA in *Brachypodium distachyon*.
1128 The Plant Cell. 25 :4363–4377,

1129 Würschum T, Boeven PHG, Langer SM, Longin CFH, Leiser WL. 2015. Multiply to
1130 conquer : Copy number variations at Ppd-B1 and Vrn-A1 facilitate global adaptation
1131 in wheat. BMC Genetics. 16:96

1132 Yan W, Wang B, Chan E, Mitchell-Olds T. 2021. Genetic architecture and adaptation of
1133 flowering time among environments. New Phytol. 230:1214–1227.

1134 Yeaman S. 2022. Evolution of polygenic traits under global vs local adaptation.
1135 Genetics 220(1) : iyab134

1136 Yeaman S, Gerstein AC, Hodgins KA, Whitlock MC. 2018. Quantifying how constraints
1137 limit the diversity of viable routes to adaptation. PLoS Genet. 14:1–25.

1138 Yeaman S, Hodgins KA, Lotterhos KE, Suren H, Nadeau S, Degner JC, Nurkowski KA,
1139 Smets P, Wang T, Gray LK, et al. 2016. Convergent local adaptation to climate in
1140 distantly related conifers. Science. 353:1431–1433.

1141 Zan Y, Carlborg Ö. 2019. A Polygenic Genetic Architecture of Flowering Time in the
1142 Worldwide Arabidopsis thaliana Population. Mol. Biol. Evol. 36:141–154.

1143 Zhang D, Abrash EB, Nunes TDG, Prados IH, Gil MXA, Jesenofsky B, Lindner H,
1144 Bergmann DC, Raissig MT. 2022. Opposite polarity programs regulate asymmetric
1145 subsidiary cell divisions in grasses. Elife 11:e79913.

1146 Zhou X, Stephens M. 2012. Genome-wide efficient mixed-model analysis for
1147 association studies. Nat. Genet. 44:821–824.